



RESEARCH ARTICLE

10.1002/2016GC006690

Key Points:

- Mantle was exhumed at the base of the sedimentary pile of the Basque-Cantabrian Basin along the Leiza detachment fault in the mid-Cretaceous
- Clumped isotopes in veins of outcropping serpentinized peridotites point to recrystallization at low T (3–49°C) from meteoric water
- Recrystallized ophicalcites in Lherz and Urdach show T of 32–42°C (from meteoric water) and up to 230°C (from saline fluid), respectively

Correspondence to:

I. DeFelipe,
defelipe@geol.uniovi.es

Citation:

DeFelipe, I., D. Pedreira, J. A. Pulgar, E. Iriarte, and M. Mendia (2017), Mantle exhumation and metamorphism in the Basque-Cantabrian Basin (N Spain): Stable and clumped isotope analysis in carbonates and comparison with ophicalcites in the North-Pyrenean Zone (Urdach and Lherz), *Geochem. Geophys. Geosyst.*, 18, 631–652, doi:10.1002/2016GC006690.

Received 21 OCT 2016

Accepted 26 JAN 2017

Accepted article online 31 JAN 2017

Published online 23 FEB 2017

Mantle exhumation and metamorphism in the Basque-Cantabrian Basin (N Spain): Stable and clumped isotope analysis in carbonates and comparison with ophicalcites in the North-Pyrenean Zone (Urdach and Lherz)

I. DeFelipe¹, D. Pedreira¹ , J. A. Pulgar¹, E. Iriarte² , and M. Mendia³

¹Departamento de Geología, Universidad de Oviedo, Oviedo, Spain, ²Departamento de Ciencias Históricas y Geografía, Universidad de Burgos, Burgos, Spain, ³Departamento de Mineralogía y Petrología, Universidad del País Vasco-E.H.U, Bilbao, Spain

Abstract The presence of ophicalcites in serpentinized peridotites together with fragments of these rocks in Cretaceous breccias along several North-Pyrenean basins led to the interpretation of complete mantle exhumation to the seafloor. The westernmost outcrop of peridotites in the Pyrenean-Cantabrian belt is located in Ziga (eastern Basque-Cantabrian Basin), associated to a band of HT metamorphism related to the Leiza fault (Marble Unit). We present a petrological and geochemical study of the marbles and Ziga peridotite-hosted calcite, including standard stable isotope composition and clumped isotope geothermometry. These isotopic techniques allow the determination of different types of formational fluids and crystallization temperatures, and are a useful tool for studying carbonation processes in hyperextended basins. Fieldwork and analytical studies lead us to conclude that during the opening of the Bay of Biscay, mantle rocks were unroofed at the base of the sedimentary pile of the eastern Basque-Cantabrian Basin. However, the ophicalcite veins were recrystallized from meteoric fluids at low temperatures ($\leq 49^\circ\text{C}$). The primary carbonate phase may have been formed either during the mid-Cretaceous unroofing of the mantle or in a post-exhumation stage. The process of mantle exhumation was accompanied with HT-LP metamorphism and fluid circulation along major faults that reset the marine isotopic signature in the nearest marbles. For comparison, ophicalcites from Urdach and Lherz (North-Pyrenean Zone) were included in the clumped isotope study. Results show that they were recrystallized from hot (~ 200 – 230°C), saline fluids, and from meteoric fluids at near ambient temperatures (~ 32 – 42°C), respectively.

1. Introduction

During the opening of the Bay of Biscay in the Cretaceous, extreme crustal thinning led to local mantle exhumation in several places along the Pyrenean realm. The crustal stretching promoted a High Temperature-Low Pressure (HT-LP) metamorphism in numerous parts of the North Pyrenean Zone (NPZ) [Golberg and Leyreloup, 1990] and in the eastern Basque-Cantabrian Basin. The highest metamorphic temperatures are measured close to the mantle exposures in the Central and Western NPZ [e.g., Clerc and Lagabrielle, 2014; Clerc et al., 2015]. Evidence of mantle exhumation is the presence of fragments of peridotites embedded in the Albian-Cenomanian breccias of several North-Pyrenean basins and the development of ophicalcites in the upper part of the peridotite bodies [e.g., Lagabrielle and Bodinier, 2008; Jammes et al., 2009; Lagabrielle et al., 2010; Clerc et al., 2013].

“Ophicalcite” is the present-day form of the term “ophicalce,” introduced by Brongniart [1813] to designate a *mélange* rock basically made up of carbonate with serpentine, talc or chlorite. It is, therefore, a descriptive term of carbonates developed in relation to ultramafic rocks and it does not strictly refer to any particular genetic process. Bonney [1879] discovered ophicalcites in the Ligurian Alps and then, ophicalcites were described in many ophiolitic sequences [Barbieri et al., 1979; Lemoine et al., 1987; Lavoie, 1997]. Ophicalcites form in a wide range of geological settings by low-temperature alteration of serpentinites in the presence of fluids. These fluids may be either uprising hydrothermal fluids or percolating marine or meteoric waters. The tectonic settings where these carbonation processes are observed *in situ* include slow spreading ridges and oceanic transform faults [Mével, 2003; Kelley et al., 2005], ocean-continent transition zones in passive

margins [Agrinier *et al.*, 1988; Milliken and Morgan, 1996; Schwarzenbach *et al.*, 2013] or even modern alteration at ambient temperatures in outcropping peridotites [Kelemen and Matter, 2008; Streit *et al.*, 2012]. In these settings, exhumed mantle rocks are thermodynamically unstable. Olivine and pyroxenes react then with fluids to form a variety of hydrous minerals such as serpentine, brucite, and talc. Pyroxene reacts faster than olivine at temperatures above 250°C releasing Ca, Si and H₂ [Bach *et al.*, 2004]. The serpentinization process generates high-pH fluids, rich in methane, which enhances the precipitation of carbonates [Trommsdorff *et al.*, 1980; Kelley *et al.*, 2005]. This carbonation process has been postulated as a promising way to store CO₂, by pumping it into weathering peridotites and promoting the precipitation of calcite [Kelemen and Matter, 2008]. The presence of fossil ophicalcites found in the Alps, the Apennines, and the Pyrenees, among other mountain chains, led to the interpretation that they were the result of hydrothermal alteration of serpentinized peridotites. For example, Lemoine *et al.* [1987] suggested that ophicalcites in the Apenninic and Alpine ophiolites developed on seafloor exposures of exhumed mantle. For the Totalp ophicalcites in the Swiss Alps, Bernoulli and Weissert [1985] proposed a tectonic fragmentation of oceanic basement rocks in a transform margin along the northern edge of the Apulian microplate before the onset of the Alpine orogeny, with infiltration of fluids and/or diagenetic sediments into the open voids. Barbieri *et al.* [1979] studying the carbon, oxygen, and strontium isotopic compositions of ophicalcites from the North-Central Apennines, suggest that the carbonate cement had a marine origin, and might have formed in a context similar to that of the Mid-Atlantic Ridge. Früh-Green *et al.* [1990], based on petrography and stable isotope data in Alpine ophicalcites, interpret the carbonate microstructures as evidence for early seafloor fragmentation, cementation and fluid activity in the Jurassic Tethys. Hence, the originally descriptive term “ophicalcite” is commonly associated at present to a particular genetic process that takes place at or very near to the seafloor.

Among the more than 40 lherzolitic bodies disseminated all along the Pyrenean chain [Monchoux, 1970; Fabriès *et al.*, 1998], ophicalcites are restricted to a few outcrops [Lagabrielle and Bodinier, 2008; Jammes *et al.*, 2009; Clerc *et al.*, 2013]. The westernmost outcrop of peridotitic rocks along the Pyrenean-Cantabrian mountain belt is located in Ziga (Navarre, Spain). It was first documented by Lamare [1936], who interpreted it as a tectonic slice of high-grade rocks cropping out along the Leiza Fault (“Nappe des Marbres”). These rocks were later studied by Walgenwitz [1976] and Mendia and Gil Ibarra [1991], but the present contribution is the first one focused on the ophicalcites themselves instead of on the peridotitic parent bodies.

Our main goal was to recognize the tectonic environments in which the Pyrenean mantle rocks were altered to form ophicalcites and the link between mantle unroofing and metamorphism in the surrounding units. In this work we present a petrographic and isotopic study of some metamorphic rocks belonging to the Marble Unit together with peridotite-hosted calcite veins from Ziga. The isotopic study includes the determination of stable carbon and oxygen compositions and the use of the clumped isotope technique, which adds key information about the type of fluids involved in the carbonation process and the temperature of carbonate (re)crystallization. Clumped isotope thermometry has been recently applied to the study of ophicalcites in Oman [Streit *et al.*, 2012; Falk *et al.*, 2016] and in the Iberia Abyssal Plain [Klein *et al.*, 2015], but to our knowledge, this is the first time it is applied to “alpine-type” ophicalcites in orogenic lherzolites. For comparison, we applied this technique also to ophicalcite samples from the Urdach and Lherz massifs, located in the western and central North Pyrenean Zone, respectively, both of them showing evidence of sedimentary reworking at the seafloor.

We aimed to use all this information to add constraints on the tectonic evolution of the eastern Basque-Cantabrian Basin during the mid-Cretaceous. Comparison of results from Ziga, Urdach, and Lherz might enlighten possible variations in the style of Mesozoic extensional tectonics affecting the North-Iberian realm before the onset of the Alpine orogeny.

2. General Tectonic Setting

The Pyrenean-Cantabrian mountain chain extends along the Northern border of the Iberian Peninsula for about 1000 km in an ~E-W direction. It is the result of the convergence between Iberia and Eurasia from Late Cretaceous to Miocene, in the context of the Alpine orogeny [Choukroune, 1976; Srivastava *et al.*, 1990; Muñoz, 1992; Vergés *et al.*, 1995; Rosenbaum *et al.*, 2002; among others]. The Alpine convergence along the northern border of Iberia resulted in continent-continent collision in the east (the Pyrenees) and shortening

and uplift of the former Mesozoic margin in the west, forming a coastal range (the Cantabrian Mountains). Previously, this area was affected by lithospheric extension during most of the Mesozoic. This episode gave rise to hyperextended rift basins with local mantle exhumation in the future Pyrenean domain, and to the opening of the Bay of Biscay to the west, in the Cantabrian domain, in relation to rifting in the North-Atlantic Ocean [Lagabriele and Bodinier, 2008; Jammes et al., 2009, 2010; Tugend et al., 2014, 2015; Pedreira et al., 2015].

A geological map of the central-western Pyrenees is shown in Figure 1, with the location of the three studied peridotite outcrops. The Pyrenean core is represented by a band of Paleozoic basement rocks affected by mainly south-vergent Alpine structures, namely the Axial Zone, and by the disconnected outcrops to the west, forming the Basque Massifs. Mesozoic and Cenozoic sedimentary rocks affected by folding and thrusting with general opposite vergences, form the Northern and Southern Pyrenean Zones (NPZ and SPZ). The NPZ is locally separated from the Axial Zone by the North-Pyrenean Fault, a deep structure that disappears toward the west of the chain and that has a controversial origin and significance [Hall and Johnson, 1986; Canérot et al., 2004]. The NPZ is a narrow band of thrust and folded sheets of mainly Mesozoic rocks, commonly detached on top of the evaporitic materials of the Triassic Keuper facies. Paleozoic basement rocks are locally exposed forming the North Pyrenean Massifs. In the NPZ, a thin band of rocks immediately north of the North-Pyrenean Fault, underwent HT-LP metamorphism during the mid to Upper Cretaceous, from 110 to 90 Ma [Albarède and Michard-Vitrac, 1978; Montigny et al., 1986; Golberg and Leyreloup, 1990; Clerc et al., 2015]. The NPZ contains the Urdach and Lherz peridotites. Urdach is located in the western termination of the northernmost thrust of a system of three thrust-and-fold units, the Chaînons Béarnais, while Lherz is located in the Aulus basin, between the Axial Zone and the North Pyrenean Massifs. Toward the north, the North-Pyrenean Zone is thrust over the Cenozoic sediments of the Aquitaine foreland basin, and is partially covered with postorogenic deposits. The south-verging Mesozoic-Cenozoic fold-and-thrust belt (South-Pyrenean Zone) is much wider and overlies the Ebro foreland basin.

Toward the western edge of the Pyrenees, the Pamplona transfer fault introduces a significant change in the structure of the orogen [Larrasoña et al., 2003a; Pedreira et al., 2003, 2007; Roca et al., 2011]. It is a major but quite diffuse accident overlined by the NNE-SSW alignment of Triassic (Keuper) salt diapirs. The origin of the Pamplona fault is thought to be related to a fracture network developed within the European basement during the latest stages of the Variscan orogeny, in the Late Carboniferous [e.g., Mattauer, 1968]. It had an important role in controlling the Cretaceous sedimentation, and constitutes the eastern limit of the

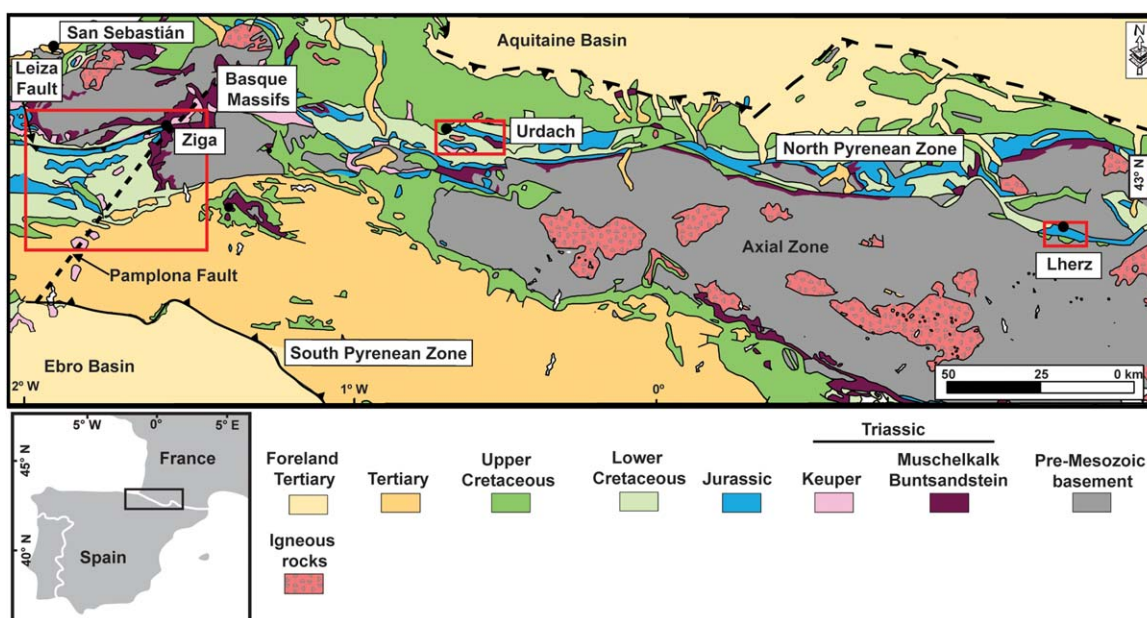


Figure 1. Simplified geological map of the western and central Pyrenees with location of the studied outcrops (after Álvaro et al. [1994]). Squares show the location of detailed maps depicted in Figures 2a, 3a, and 3d.

Basque-Cantabrian Basin, presently inverted and incorporated into the Pyrenean-Cantabrian belt. Partitioning of deformation also occurred during the tectonic inversion at a crustal scale, and structures with opposing vergences can be observed on both sides along part of its trace. West of this structure, the E-W trending Leiza Fault (Figure 1) represents another deep structure with an associated band of HT-LP metamorphism, in this case to the south of the fault trace; namely the “Nappe des Marbres” or “Marble Unit” [Lamare, 1936]. This fault was a normal fault or extensional detachment during the Mesozoic, later inverted as a north-verging thrust during the Alpine contractional deformation. Several high-grade rocks such as granulites and migmatites crop out along the trace of the Leiza Fault, including the peridotites of Ziga at the junction with the Pamplona Fault [Mendia and Gil Ibarbuchi, 1991], which form small outcrops (less than $\sim 10 \text{ m}^3$ in total volume).

3. Geological Setting of the Studied Outcrops

3.1. Eastern Basque-Cantabrian Basin

A geological map of the area studied is depicted in Figures 1 and 2. In this area, the Pamplona fault separates the Paleozoic massifs of Cinco Villas to the west and Alduides to the east. Two other major faults, E-W oriented, run parallel to the southern border of Cinco Villas: the Ollín Thrust, which uplifts the Paleozoic massif on top of a Cretaceous basin known as “Central Depression”; and the Leiza Fault, which thrusts the southern block over the Central Depression. South of this thrust fault, a band of calcareous Triassic to Lower Cretaceous rocks exhibits the metamorphism of the “Marble Unit”, which developed under conditions of 500°C and 3 kbar based on calibration from mineral associations [Martínez-Torres, 2008]. The age of this metamorphism has been thoroughly discussed. Albarède and Michard-Vitrac [1978] dated a metamorphic phlogopite close to Ziga and obtained ages of $82.6 \pm 0.5 \text{ Ma}$ and $101 \pm 16 \text{ Ma}$ with the $^{39}\text{Ar}\text{-}^{40}\text{Ar}$ and $^{87}\text{Rb}\text{-}^{87}\text{Sr}$ methods, respectively. Montigny et al. [1986] analyzed another phlogopite and a biotite with the K-Ar method, obtaining ages of $93 \pm 3 \text{ Ma}$, and $81 \pm 3 \text{ Ma}$, respectively. Geological evidence, such as fragments of marble included in breccias of Turonian-Coniacian age, date the metamorphic event as at

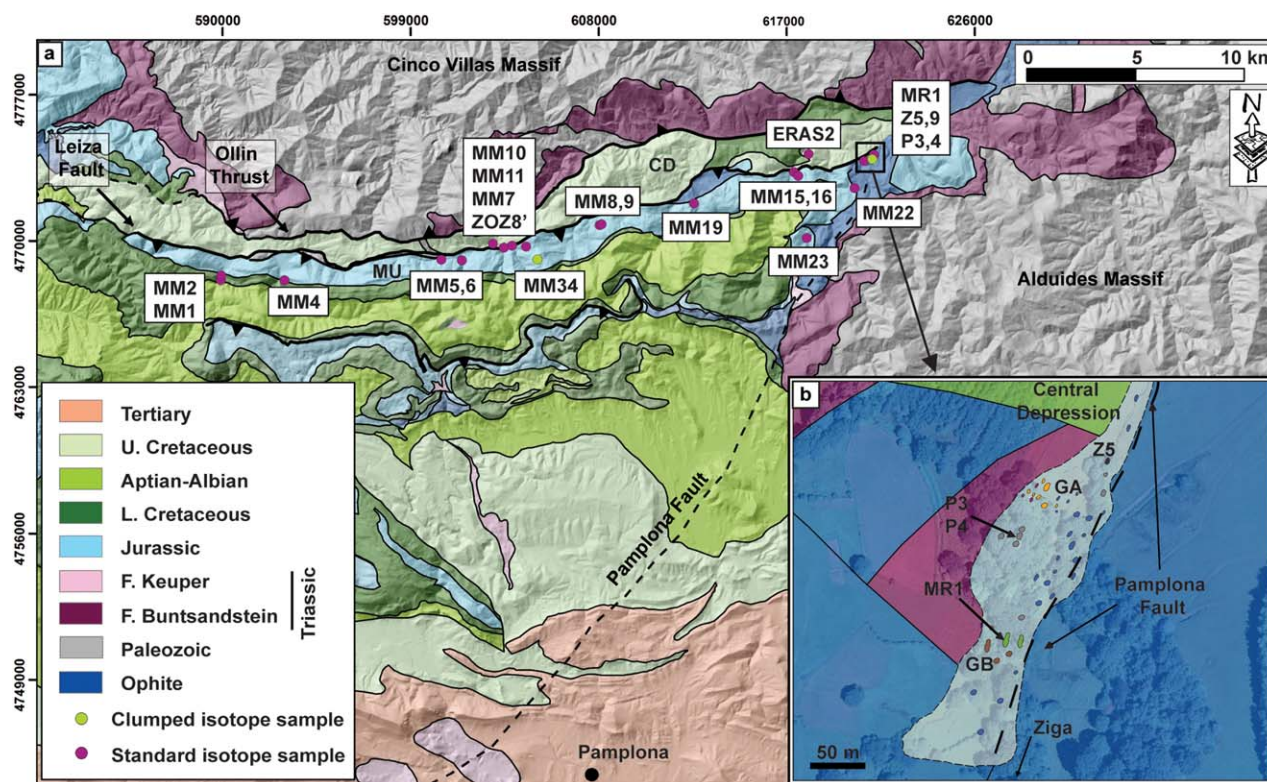


Figure 2. (a) Regional geological map of the westernmost Pyrenees and eastern Basque-Cantabrian Basin with the location of the analyzed samples. CD: Central Depression, MU: Marble Unit (after Del Valle et al. [1973], Carbayo et al. [1977], Gabaldón et al. [1983, 1984]) and (b) a detailed map of the Ziga mélangé, where the largest exotic blocks are mapped.

least partly pre-Turonian and possibly late Cenomanian [Mathey et al., 1999; Iriarte, 2004]. Associated with the metamorphism, a hydrothermal event also produced recrystallizations in the Albian to Upper Turonian-Coniacian materials of the Central Depression [Iriarte, 2004].

The trace of the Leiza fault is marked by a series of outcropping slices of mid-lower crustal rocks, the mantle rocks being restricted to the junction between the Leiza and Pamplona faults, near the village of Ziga (Navarre, Spain) [Mendia and Gil Ibarra, 1991]. These mantle rocks show up as exotic, metric-size blocks of serpentinized lherzolites embedded in a clayey-gypsum matrix, together with other blocks of acid and basic granulites, marbles, subvolcanic basic rocks ("ophites"), and Buntsandstein-facies Triassic sandstones [DeFelipe et al., 2012a, 2012b]. This complex unit, with unfavorable exposure conditions, was referred to as "Écaille de Ciga" (Ciga -or Ziga- slice) by Walgenwitz [1976]. We prefer the more descriptive term of "Ziga mélange." This mélange is approximately 100 m wide and 350 m long, and it is elongated in the direction of the Pamplona Fault (Figure 2b). The matrix of this mélange is rich in clay minerals, gypsum, carbonates, quartz, and muscovite. Comparable mineralogy is found in several Keuper facies evaporitic diapirs cropping out along the Pamplona Fault, like the Estella diapir (located in the junction with the E-W trending South Pyrenean Frontal Thrust), which also contains blocks of basic and acid igneous rocks, gneisses and marbles [Pflug, 1973].

3.2. Urdach and Lherz Ophicalcites

The ophicalcites sampled in this work for the isotopic comparison with the Ziga ones, belong to the Col d'Urdach massif and the Étang de Lherz massif.

The Urdach outcrop is located in the easternmost margin of the Mauléon basin (French Western Pyrenees) and was first described by Monchoux [1970], who named it as Urdach-Les Pernes massif. The peridotitic bodies crop out at several points along the Chaînons Béarnais unit, formed by a succession of three E-W trending parallel thrust sheets over a lubricating sole of late Triassic salts and clays and exposing the Mesozoic carbonates [Canérot and Delavaux, 1986]. The Urdach peridotitic body (Figure 3b), is a 1.5 km wide

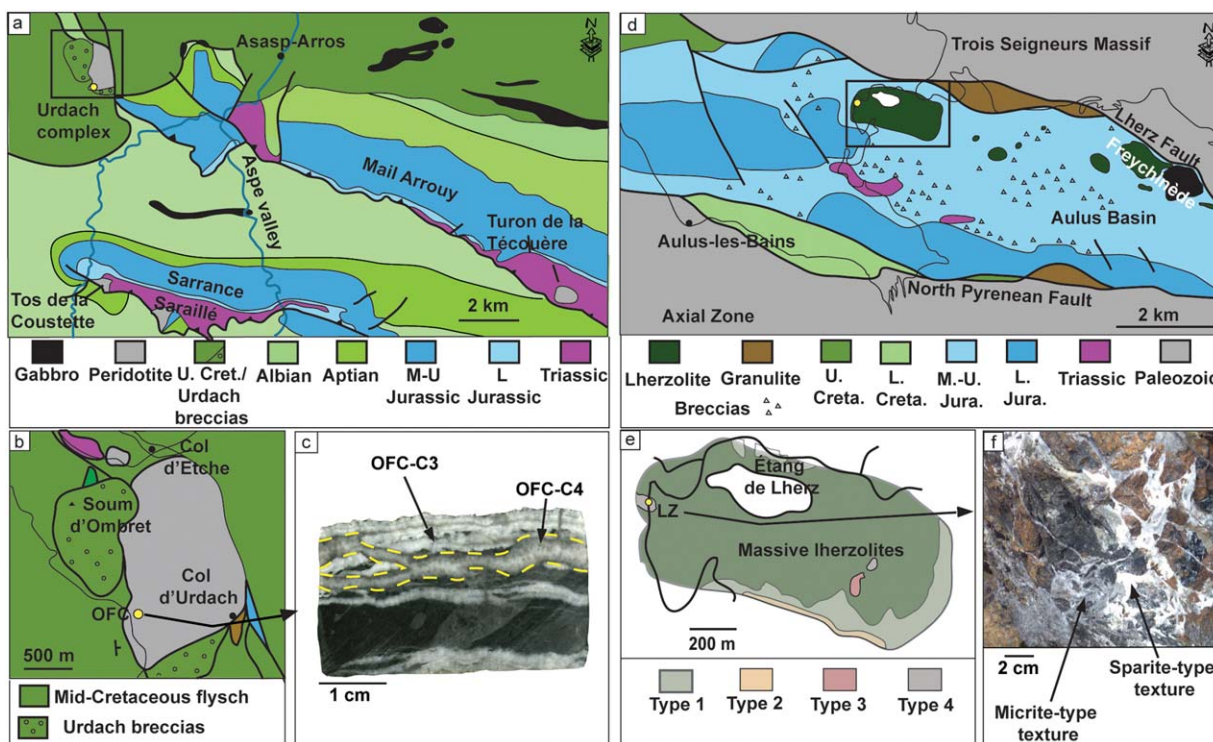


Figure 3. (a) Geological map of the northern part of the Chaînons Béarnais (modified from Lagabrielle et al. [2010]). (b) Detailed map of the Urdach complex (modified from Lagabrielle et al. [2010]) with the location of the samples OFC. (c) Hand sample from Urdach with location of analyzed veins. (d) Geological map of the Aulus Basin (after Lagabrielle and Bodinier [2008]). (e) Detailed map of the Lherz massif with the four types of breccias defined by Lagabrielle and Bodinier [2008] and location of the LZ samples. (f) Detail of the Lherz hand sample with both types of textures identified.

peridotite slice located at the western end of the northernmost thrust sheet, the Mail Arrouy. The outcrop is formed by highly serpentized lherzolites capped locally by an important development of calcite veins with typical opicalcite texture [Jammes *et al.*, 2009] (Figure 3c). It is overlain by a large volume of Upper Albian-Cenomanian sedimentary breccias composed of fragments of dominant Paleozoic basement and highly serpentized peridotite, the so-called “Urdach breccias” [Casteras, 1970; Souquet *et al.*, 1985]. The opicalcite from Urdach sampled for this work belongs to the western part of that massif, in the Bilatre quarry, very close to the Albo-Cenomanian breccias of the Soum d’Ombret.

Jammes *et al.* [2009] and Lagabrielle *et al.* [2010] propose models of hyperextended crust in which low-angle detachment faults led to exhumation of mantle rocks to the seafloor as enlightened by the occurrence of opicalcites locally capping the lherzolites, and the presence of lherzolite fragments within the Urdach breccias [e.g., Fortané *et al.*, 1986; Duée *et al.*, 1984; Jammes *et al.*, 2009]. Debros *et al.* [2010], however, argue that the Urdach breccias are separated mechanically from the lherzolite body and consider that they represent autochthonous fault-scarp deposits related to a synsedimentary transverse fault, which would also provide the path for fluids to develop the opicalcites.

The lherzolites of the Étang de Lherz massif (the type locality of lherzolites) are located in the central-eastern part of the North Pyrenean Zone (Figures 1 and 3d). They crop out in a small and narrow Mesozoic basin (the Aulus basin), WNW-ESE trending, limited by two subvertical faults that mark the boundary with the Axial Zone to the south and with the Trois Seigneurs Massif to the north. This basin is mainly filled with a series of carbonate rocks of Jurassic to Lower Albian age that suffered a HT-LP metamorphism characterized by temperatures of 450–600°C [Clerc and Lagabrielle, 2014], maximum pressures of 3 kb [Ternet *et al.*, 1997] and dated between 110 and 85 Ma [Albarède and Michard-Vitrac, 1978; Montigny *et al.*, 1986]. Lherzolites appear as blocks of variable sizes (up to kilometric scale) surrounded by voluminous breccia formations [Clerc *et al.*, 2013]. The breccias exposed around the main body of Étang de Lherz have been classified in 4 types by Lagabrielle and Bodinier [2008] (Figure 3e): monomictic breccias composed of peridotite clasts, with cataclastic characteristics (Type 1); similar breccias but with sedimentary reworking and including carbonate clasts (Type 2); ultramafic sandstones with blocks of lherzolite and isolated serpentine clasts (Type 3); and clastic rocks resembling the opicalcites of the Apenninic and Alpine ophiolites [Lemoine *et al.*, 1987], with late carbonate veins (Type 4). Except for Type 1, Lagabrielle and Bodinier [2008] call for a sedimentary origin or reworking for these breccias. The opicalcite from Lherz studied in this work was taken along the road at site LHZ 8 of Lagabrielle and Bodinier [2008] (Figure 3f) and corresponds to their “Type 4” breccias.

Clerc *et al.* [2013] present a petrographical and geochemical study of several Pyrenean opicalcites, including samples from Urdach and Lherz. Based on their oxygen and carbon stable isotopic signatures, these authors conclude that the Pyrenean opicalcites may be the product of three different processes: (i) deep and hot hydrothermal activity; (ii) tectonic fracturing and cooler hydrothermal activity; and (iii) sedimentary processes leading to cogenetic associations of calcite veins with polymictic breccias after exposure of subcontinental mantle to the floor of the basins. According to that study, the Urdach opicalcites belong to the second type, whereas the Lherz opicalcites belong to the third one.

4. Study Techniques, Sample Selection, and Methods

A mineralogical study combining X-Ray diffraction (XRD), petrographic microscopy, cathodoluminescence (CL), SEM, and stable isotope geochemistry of the main carbonate rocks has been carried out in order to establish their mineralogy, patterns of alteration, and different crystallization phases. XRD was used to distinguish varieties of serpentine in the peridotites and the mineralogy of the Ziga *mélange* matrix. A total of 56 stable isotope analyses in carbonates were carried out in the facilities of the Universities of Oviedo Barcelona, and the Stable Isotope Laboratory of the Swiss Federal Institute of Technology in Zürich (ETH). Among these, 15 correspond to carbonate veins of the peridotites from the Ziga *mélange*, 24 to the carbonate samples cropping out along the Leiza fault, 15 microdrillings to the Urdach opicalcites, and 2 to the Lherz samples.

In order to obtain the isotopic signatures, each carbonate sample was dissolved in 100% H₃PO₄ at a constant temperature of 25°C to extract the CO₂ gas [McCrea, 1950], which was analyzed in a mass spectrometer, following the procedure described in Stoll *et al.* [2015]. Results are expressed using the conventional $\delta^{18}\text{O}$ and $\delta^{13}\text{C}$ notation with respect to the Pee Dee Belemnite (PDB) standard.

Clumped isotope analyses were performed following the procedure described by Schmid and Bernasconi [2010]. Sample CO₂ is extracted by reaction of carbonate powder at 70°C with ~103% phosphoric acid for 180 s and is then frozen with liquid nitrogen for cryogenic purification to be finally released into a Thermo Fisher Scientific Kiel IV mass spectrometer at 30°C. Isotopic results for the mineral phases are presented in the normal δ notation relative to the PDB standard, whereas the calculated fluid $\delta^{18}\text{O}$ values are expressed relative to the Standard Mean Ocean Water (SMOW). This technique combines the standard stable isotope geochemistry in carbonates with paleothermometry and takes advantage of the temperature dependence of the degree of “clumping” of ¹³C–¹⁸O bonds to each other according to a theoretical random distribution [Ghosh *et al.*, 2006; Eiler, 2007]. The measured mass-47 (mainly ¹³C¹⁸O¹⁶O with minor ¹²C¹⁸O¹⁷O and ¹³C¹⁷O₂) is compared to that expected for a stochastic distribution and the difference is denoted as Δ_{47} . The values of Δ_{47} are dependent on the temperature of crystal growth and independent of bulk isotopic composition. This provides the opportunity to determine temperature of precipitation (or recrystallization) and at the same time to calculate the $\delta^{18}\text{O}$ of the formational fluid [Grauel, 2012]. In the case of recrystallization, however, we must be aware that the clumped isotope temperatures would reflect the temperature of recrystallization (i.e., a reordering of the clumped isotopes) and therefore some caution is needed when interpreting these temperatures and the values of $\delta^{18}\text{O}$ obtained for the fluid. Considering this caveat and the required assumption of thermodynamic equilibrium, clumped isotopes have proved to be highly efficient in preserving the information of successive crystallization events even after heating the samples at ~100–115°C for 10⁶–10⁸ yr time scales [Henkes *et al.*, 2014]. This means that we can potentially keep the record of the prediagenetic/diagenetic processes or fault cementation history, preserved even within the same specimen [e.g., Huntington *et al.*, 2011; Loyd *et al.*, 2012; Swanson *et al.*, 2012].

5. Description of the Samples

5.1. Field and Macroscopic Aspects

5.1.1. Ziga *Mélange*

The Ziga *mélange* forms a poorly defined unit made up of a few outcrops due to the dense vegetation cover in the area. The matrix is formed by a white-yellowish crumbling mass of mainly fine-grained gypsum and phyllosilicates with idiomorphic and millimetric to centimetric crystals of pyrite disseminated throughout. Within this matrix, millimetric to metric fragments of different types of rocks are found, including Triassic sandstones, marbles, acid and basic granulites, and peridotites. A photograph of the Ziga *mélange* containing one of the largest blocks of marble is depicted in Figure 4a, and details of the matrix and marble are shown in Figures 4b and 4c, respectively.

Ziga lherzolites form up to meter-sized outcrops within the gypsum matrix. Within the peridotite, numerous veins and veinlets give these rocks a brecciated aspect. In these samples, two types of carbonate texture have been identified: veins of calcite in rather massive blocks of serpentized lherzolites (hereafter referred to simply as “ophicalcites”, Figures 4d and 4e) and veins in more brecciated samples of serpentized lherzolites (hereafter referred to as “ophicalcite breccias,” Figure 4f). The ophicalcites are formed by millimetric veins of white calcite that develop over a greenish mass of serpentinite and ferromagnesian minerals. The ophicalcite breccia has a crumbly aspect of serpentinite fragments, remnants of the primary lherzolite mineralogy as well as veins and patches of calcite. These two types of calcite veins have not been identified either in the matrix or in the rest of the blocks.

5.1.2. Marble Unit and Central Depression

The Marble Unit comprises a wide variety of pre and syn-rift sedimentary rocks. Outcropping lithologies are Lower Jurassic limestone breccias, Jurassic to Lower Cretaceous limestones and mid-Cretaceous silt and sandstone. These lithologies are metamorphosed close to the Leiza fault. The metamorphic imprint is almost negligible in the western part of the Marble Unit, it reaches its maximum in the central-eastern part and diminishes toward the eastern termination [Martínez-Torres, 2008]. Figure 4g depicts sample MM34 which is a Lower Cretaceous breccia marble made up of heterometric, monogenic and subrounded millimetric and centimetric-size carbonate clasts in a fine-grained matrix.

The Central Depression is mainly composed of Cretaceous sedimentary rocks, namely mid-Cretaceous limestones and sandstones, and typical Upper Cretaceous flysch facies [Iriarte, 2004; Bodego *et al.*, 2015]. Lower Albian to Upper Turonian limestones and sandstones present signs of hydrothermalism such as growth of authigenic quartz crystals, calcite fracture-sealing and matrix neomorphism. Iriarte [2004] and Iriarte *et al.*

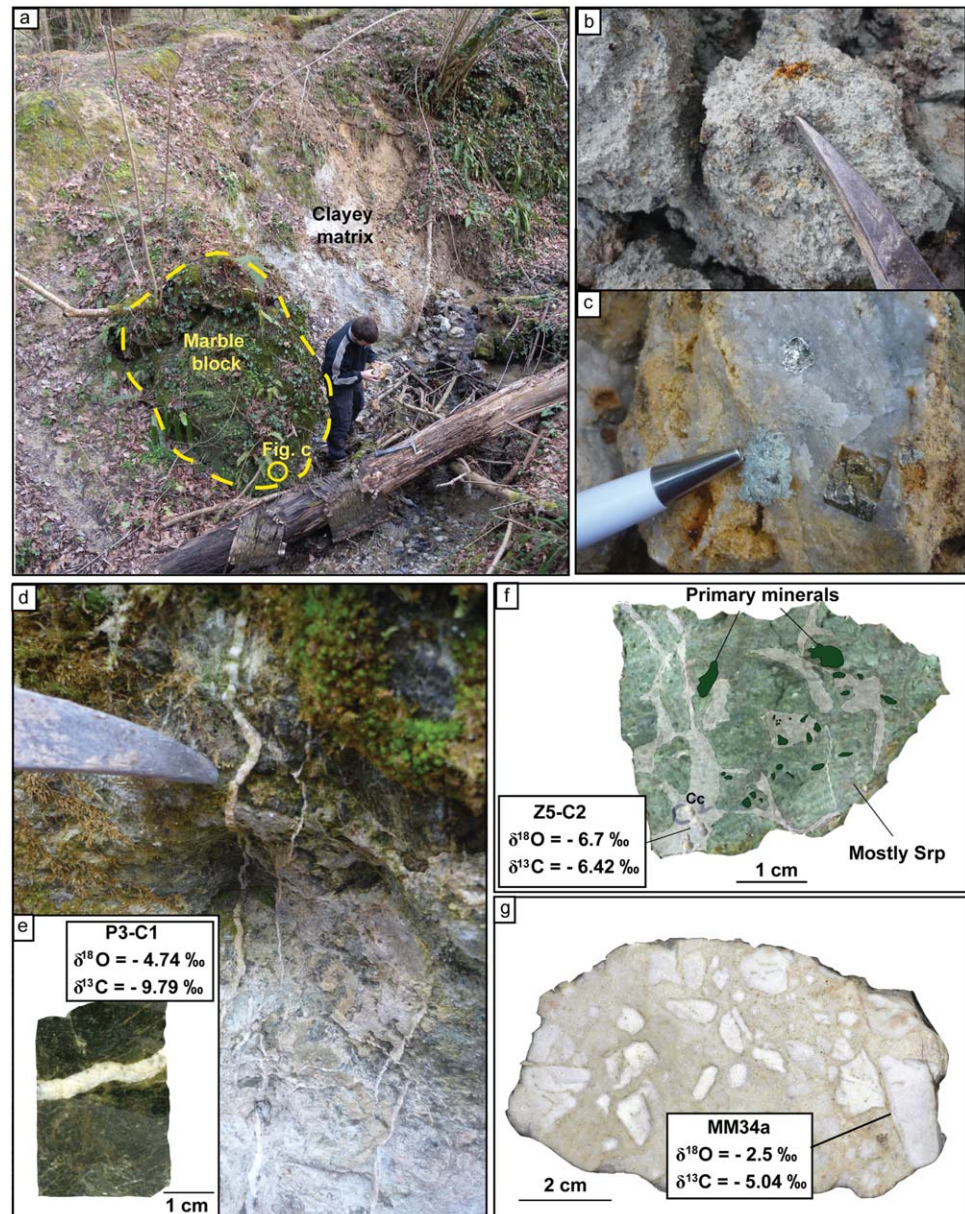


Figure 4. (a) General view of the Ziga *mélangé* including the biggest block of marble. (b) Detail of a hand sample of the *mélangé* matrix. (c) Detail of the marble in the Ziga *mélangé* (MR1 sample); a fine-grained altered and crumbly marble with growth of idiomorphic crystals of pyrite. (d) Altered peridotite with veins of calcite in the Ziga *mélangé*. These types of calcite veins have not been identified either in the matrix or in the rest of the blocks. (e) Detail of the calcite vein in the Ziga peridotite (P3-C1). (f) Hand sample of the ophicalcite breccia within the Ziga *mélangé* (Z5-C2) (Srp: serpentine; Cc: calcite; Primary minerals include mainly olivine, pyroxene and spinel). (g) Hand sample of the marble breccia belonging to the Marble Unit (MM34). See location in Figure 2.

[2011] argue that the hydrothermalism is concentrated mainly in two events: in the Upper Albian and the Upper Turonian. This conclusion is based on stratigraphic and petrographic observations and fluid inclusion analyses in authigenic minerals of Lower Albian to Upper Turonian rocks from the Central Depression.

5.1.3. Urdach and Lherz Ophicalcites

Urdach ophicalcites are fundamentally made up of millimetric to decimetric veins of calcite filling up fractures within the peridotitic rocks. Figure 3c depicts an Urdach ophicalcite sample with abundant veins filling fractures with constant, repeated orientations. Several families of veins can be distinguished, with a first phase forming the thickest veins by coalescence of numerous veinlets (OFC-C3 in Figure 3c); a later family with white-grayish calcite (OFC-C4 in Figure 3c) and a final one, crosscutting the previous groups with

thinner and more disperse veins. Microdrilling was performed in the first family of veins (12 drillings) and in the second one (3 drillings).

Lherz ophicalcites, collected in the Étang de Lherz area, correspond to the “Type 4” breccias described by *Lagabrielle and Bodinier* [2008]. Clear white calcite with sparitic texture forms veins that fill fractures within the peridotite, giving it a brecciated texture. The micrite texture is described by *Clerc et al.* [2013] as a matrix-supported microbreccia as it includes heterometric and angular fragments of serpentinite and remnants of the primary mineralogy (Figure 3f). Two microdrillings were carried out, one on each calcite texture (LZ1 for the sparite and LZ2 for the micrite).

5.2. Microscopic Description

5.2.1. Ziga *Mélange*

The Ziga *mélange* matrix shows a fine-grained mass of gypsum, quartz, carbonates, and phyllosilicates (Figure 5a): kaolinite, montmorillonite, muscovite, and clinocllore. In addition, XRD analysis in one of the four samples analyzed pointed to the presence of enstatite and sanidine.

Sample MR1 is the marble collected in a metric-size block within the Ziga *mélange* (Figure 5b). It is mostly made up of calcite and dolomite in rounded and equidimensional crystals with abundant inclusions. Within the carbonate matrix, idiomorphic crystals of phyllosilicates are common. In addition, the matrix contains crystals of pyrite up to a few centimeters in size.

The ultramafic rocks in Ziga were originally lherzolites made of primary enstatite and diopside, forsterite-rich olivine, spinel, and minor amphibole. These rocks appear highly serpentized (up to 80%), with secondary chrysotile and antigorite. Carbonation overprints serpentinite as veins mostly made of calcite with minor aragonite and micritic patches. In one sample, ankerite was detected in XRD analysis. Under the microscope, vein-filling shows a mosaic texture with inequigranular and nonsystematically oriented crystals. CL images show an important recrystallization event that has preserved the original geochemistry but not the mineralogy (Figures 5c and 5d). SEM images show a previous mineralogy within the calcite veins as relicts of radial crystals of aragonite with significant amounts of Sr (up to 2.07% in weight) (Figure 5e). The ophicalcite breccia of Ziga is presented in Figure 5f. It is formed of angular, inequigranular fragments of serpentine and remnants of the previous mineralogy embedded in a carbonate matrix of sparry calcite. XRD analysis points to the presence of chrysotile as the variety of serpentine, as well as montmorillonite, a typical mineral of the *mélange* matrix. Carbonate veinlets as well as patch-filling voids have been identified in some samples. Veins of calcite show the same mosaic texture of sparry calcite crystals than the Ziga ophicalcite.

5.2.2. Marble Unit

Carbonates from the Marble Unit contain minor phyllosilicates (biotite, muscovite, phlogopite, and chlorite) and occasionally porphyroblasts of scapolite, vesuvianite, tremolite, and other amphiboles. *Llanos* [1983] also describes the presence of up to 5% in volume of talc in several marbles. Marble textures recognized in this area vary from a nematoblastic with planar oriented grains of calcite, to porphyroblastic with growth of synkinematic crystals of tremolite or vesuvianite and strain shadows (Figure 5g) and to granoblastic with equidimensional grains and triple junctions.

In thin section, clasts of the marble breccia (MM34) contain fine-grained equigranular and equidimensional carbonate crystals with very diffuse borders. The matrix has the same mineralogy with similar equigranular clasts of carbonate coexisting with finely grained recrystallized calcite (Figure 5h).

5.2.3. North-Pyrenean Ophicalcites

The Urdach peridotite is a lherzolite that is up to 80% serpentized [*Fabriès et al.*, 1998], with medium and low-temperature serpentine varieties: chrysotile and lizardite. Carbonate veins are locally intensely developed with local growth of microcrystals of pyrite. CL images show a variable grade of replacement depending on the type of vein. The largest, corresponding to the first two generations of veins, are highly recrystallized, commonly showing an alignment of inclusions that define the borders of previous minerals. A general trend of symmetrical crystal growth towards the center of the vein is recognized (Figures 6a and 6b). Later and smaller veins are less replaced. Replacement textures of serpentine by calcite and crosscutting relationships between different generations of veins are clearly recognized by SEM (Figure 6c). *Clerc et al.* [2013] also describe the crack-seal pattern of the calcite veins and their recrystallization.

The Lherz ophicalcites develop over highly serpentized lherzolites originally composed of olivine, enstatite, diopside, and Cr-spinel. These rocks show significant growth of carbonate phases grouped in two main

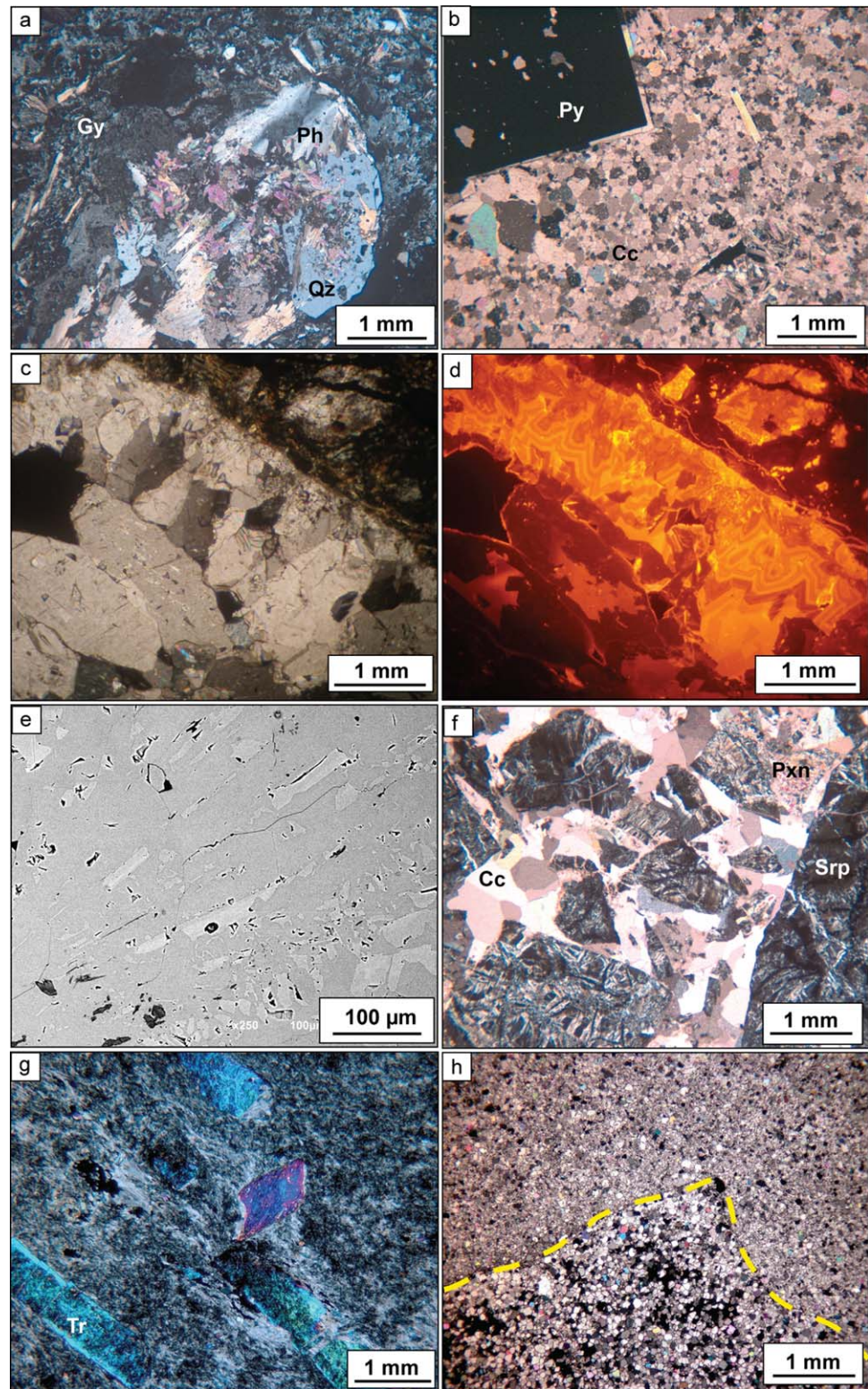


Figure 5. Petrographic microscope images (crossed nicols) of: (a) the matrix of the Ziga *mélangé* (Gy: gypsum, Qz: quartz, Ph: phyllosilicates), and (b) The marble embedded in the Ziga *mélangé* (Py: pyrite, Cc: calcite). (c and d) Petrographic image and CL image, respectively, of the same sparry calcite vein from the P3-C1 sample. The extent of recrystallization is observed in the CL image. (e) SEM image of a calcite vein from Ziga, showing relicts of radial aragonite. (f) The ophicalcite breccia (Cc: calcite, Srp: serpentine, Pxn: pyroxene). (g) Marble with porphyroblastic texture and synkinematic crystals of tremolite (Tr). (h) Marble breccia (MM34).

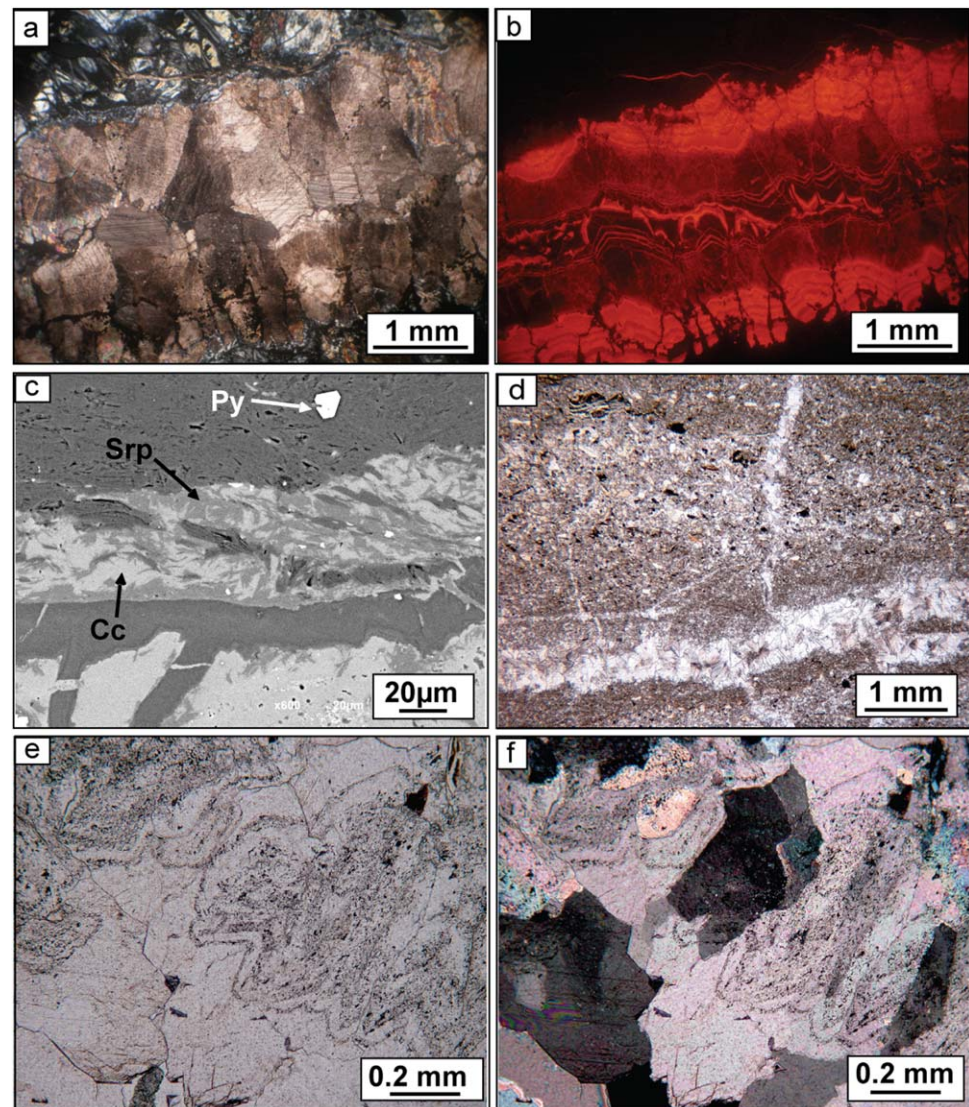


Figure 6. (a and b) Petrographic microscope image (crossed nicols) and CL image, respectively, of the same calcite vein from the OFC-C3 sample. Partly recrystallized veins show in CL a symmetric seal-crack growth, and textural differences are recognized. (c) SEM image of a calcite vein from the Urdach ophicalcite showing replacement textures of serpentine growing in the borders of the primary minerals and calcite replacing this serpentine (Py: pyrite, Srp: serpentine, Cc: calcite). (d–f) Lherz samples under the petrographic microscope showing micritic and sparitic textures ((d) parallel nicols) and recrystallization of sparry calcite, with ghosts of a previous carbonate phase ((e) parallel nicols; (f) same image with crossed nicols).

textures: micrite and sparite (Figure 6d). The micrite is the matrix of a microbreccia previously defined by *Clerc et al.* [2013], embedding fragments of carbonate minerals, serpentinite and also fresh ultramafic clasts, which gives the breccia a dusty aspect. In addition, sparite fills voids and fractures as subidiomorphic crystals showing crack-seal geometries with symmetrical growths and generally crosscutting the microbreccia phase. Under the petrographic microscope, calcite is seen as clearly recrystallized with calcite dogtooth ghosts of previous minerals as alignment of inclusions, and bigger equigranular neoformed minerals (Figures 6e and 6f). *Clerc et al.* [2013] also recognized this recrystallization under a cathodoluminescence microscope, mainly in the sparitic texture.

6. Isotopic Results

Values of $\delta^{18}\text{O}$ versus $\delta^{13}\text{C}$ for all the carbonates analyzed are presented in Table 1 and in Figure 7 together with the average values for Mesozoic marine limestones [*Keith and Weber, 1964*]. Figures 7b and 7c

Table 1. Stable and Clumped Isotope Data of the Samples Studied^a

Location	Sample	Type	$\delta^{13}\text{C}$	$\delta^{18}\text{O}$	Δ_{47}	T	T SE	$\delta^{18}\text{O}_f$	Easting	Northing
Ziga	P2-C1	Cc vein	-12.39	-4.54					616401	4775566
Ziga	P2-C2	Cc vein	-11.43	-4.79					616401	4775566
Ziga	P2-C2b	Cc vein	-12.82	-4.54					616401	4775566
Ziga	P3-C1	Cc vein	-9.79	-4.74					616396	4775553
Ziga	P3-C2	Cc vein	-10.15	-4.47					616396	4775553
Ziga	P3-C3	Cc vein	-9.98	-4.54					616396	4775553
Ziga	P3-C4	Cc vein	-12.56	-4.67					616396	4775553
Ziga	P3-C4b	Cc vein	-12.44	-4.49					616396	4775553
Ziga	P4-C1	Cc vein	-11.80	-4.64					616383	4775561
Ziga	P4-C1b	Cc vein	-11.87	-4.52					616383	4775561
Ziga	P4-C1c	Cc vein	-11.53	-4.65	0.790	6	1.5	-11.34	616383	4775561
Ziga	P3-C1b	Cc vein	-8.85	-4.58	0.804	3	1.1	-12.28	616396	4775553
Ziga	Z5-C1	Breccia	-4.38	-6.95					616467	4775621
Ziga	Z5-C2	Breccia	-6.42	-6.70					616472	4775628
Ziga	Z5-C2b	Breccia	-6.62	-6.17	0.647	49	37.3	-2.07	616472	4775628
Ziga	MR1	Marble	-4.59	-10.82					616399	4775476
Ziga	MR2	Marble	-5.08	-9.5					616388	4775478
Urdach _A	OFC-C1	Cc vein	1.3	-7.19					689189	4776596
Urdach _A	OFC-C2	Cc vein	-0.15	-10.12					689195	4776596
Urdach _A	OFC-C3	Cc vein	0.64	-7.98					689205	4776604
Urdach _A	OFC-C3b	Cc vein	0.32	-8.88	0.413	207	59.7	11.98	689205	4776604
Urdach _B	OFC-C4	Cc vein	-5.24	-4.04					689189	4776596
Urdach _B	OFC-C4b	Cc vein	-1.98	-4.34					689189	4776596
Urdach _B	OFC-C4c	Cc vein	-2.34	-4.16	0.396	229	44.3	17.91	689189	4776596
Urdach _A	OFC-C5	Cc vein	-1.11	-10.63					689203	4776597
Urdach _A	OFC-C5b	Cc vein	-1.23	-10.99					689203	4776597
Urdach _A	OFC-C6	Cc vein	-0.87	-10.39					689189	4776596
Urdach _A	OFC-C6b	Cc vein	-0.88	-10.42					689189	4776596
Urdach _A	OFC-C7	Cc vein	0.64	-8.53					689189	4776596
Urdach _A	OFC-C7b	Cc vein	0.8	-7.16					689189	4776596
Urdach _A	OFC-C8	Cc vein	-0.47	-9.84					689189	4776596
Urdach _A	OFC-C8b	Cc vein	-0.17	-9.32					689189	4776596
Lherz	LZ 1	Cc sparite	-0.7	-9.32	0.667	42	13.2	-6.67	366812	4740682
Lherz	LZ 2	Cc micrite	-1.11	-5.58	0.697	32	6	-5.23	366812	4740682
MU	MM 1	Cc	2.23	-5.43					585165	4769422
MU	MM 2	Cc	-0.83	-7.34					585154	4769690
MU	MM 4	Cc	1.37	-6.42					588217	4769523
MU	MM 5	Cc	1.54	-5.68					595696	4770541
MU	MM 6	Cc	-0.96	-6.67					596714	4770388
MU	MM 7	Cc	0.81	-5.21					599742	4771068
MU	MM 8	Cc	1.2	-6.3					603267	4772070
MU	MM 9	Cc	1.07	-5.26					603480	4772118
MU	MM 10	Cc	1.97	-7.22					599136	4771090
MU	MM 11a	Cc	2.7	-7.45					598788	4770986
MU	MM 11b	Cc	2.14	-7.28					598788	4770986
MU	MM 15a	Cc	2.43	-7.16					612512	4774678
MU	MM 15b	Cc	0.16	-7.14					612512	4774678
MU	MM 16	Cc	-3.14	-5.41					612825	4774364
MU	MM 19	Cc	-1.57	-5.73					607705	4773041
MU	MM 22a	Cc	-2.53	-6.2					615473	4773877
MU	MM 22b	Cc	-3.81	-8.81					615473	4773877
MU	MM 23	Cc	0.97	-7.61					613174	4771473
MU	Z9	Cc	1.53	-6.38					615856	4775131
MU	MM34a	Cc breccia matrix	-5.04	-2.5	0.589	74	88	3.37	600303	4770428
CD	ERAS 2	Cc	2.05	-7.19					613268	4775502
CD	ZOZ 8'	Cc	0.18	-5.78					598166	4771210

^aIsotopic values for minerals are expressed in ‰ related to the PDB standard, while the oxygen signature of the fluid is expressed versus SMOW standard. Temperature is calculated using the ETH (2013) calibration and expressed in °C and the standard error (SE). Easting and Northing are UTM-Zone30 coordinates, except for the Lherz samples, which are in UTM-Zone31. MU: Marble Unit and CD: Central Depression. Subscripts A and B in Urdach samples refer to the two groups of Figure 7a.

represent the results obtained by the clumped isotope technique, including a $\delta^{18}\text{O}$ versus $\delta^{13}\text{C}$ plot and $\delta^{18}\text{O}_{\text{fluid}}$ versus T plot, assuming that the recorded temperature is that of the last crystallization event and that it occurred under thermodynamic equilibrium. The Ziga ophicalcites show the lowest values of $\delta^{13}\text{C}$, from -12.8 to -8.8 ‰ with the $\delta^{18}\text{O}$ clustered around -4.5 ‰. The ophicalcite breccia samples show slight

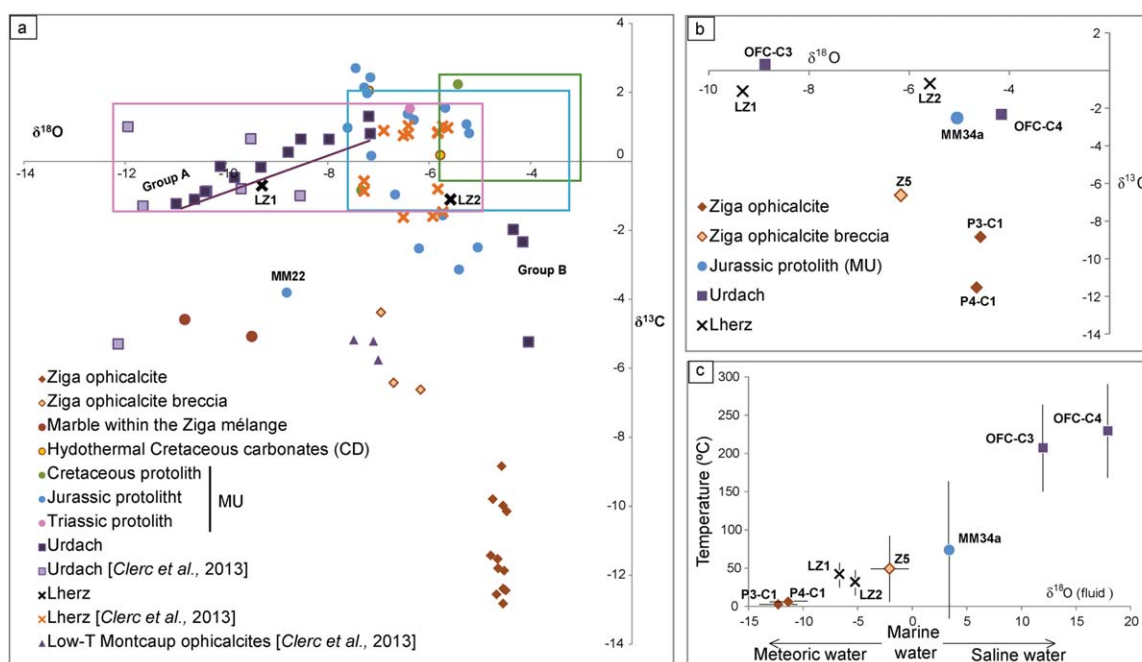


Figure 7. (a) $\delta^{18}\text{O}$ versus $\delta^{13}\text{C}$ of carbonate samples analyzed including values taken from Clerc et al. [2013] (converted from SMOW values). Pink, blue and green rectangles: average values for Triassic, Jurassic and Cretaceous marine limestones, respectively [Keith and Weber, 1964]. (b) $\delta^{18}\text{O}$ versus $\delta^{13}\text{C}$ of ophtalcites and marble analyzed in the ETH. (c) T versus $\delta^{18}\text{O}$ (fluid) estimated by clumped isotopes for the samples in b). CD: Central Depression. MU: Marble Unit.

differences, with higher $\delta^{13}\text{C}$ and lower $\delta^{18}\text{O}$ (Figures 7a and 7b). Temperatures deduced from clumped isotopes are low: less than 10°C for the ophtalcites and around 50°C for the ophtalcite breccia (this last sample has a large standard error of 37.3°C). The oxygen isotopic signature of the fluid from which the calcite precipitated is around -12‰ for the ophtalcite and close to -2‰ for the breccia (Figure 7c). The two samples of the marble within the *mélange* show $\delta^{13}\text{C}$ values of -5.1‰ and -4.6‰ and $\delta^{18}\text{O}$ values of -10.8‰ and -9.5‰ . In the Marble Unit, values fall within or close to those of marine limestones. The matrix of the marble breccia close to the Leiza Fault (sample MM34a) shows an isotopic composition that leans toward lower $\delta^{18}\text{O}$ and $\delta^{13}\text{C}$ values than Jurassic marine limestones [Keith and Weber, 1964]. The clumped isotope results for this sample yield a $\delta^{18}\text{O}_{\text{fluid}}$ of 3.4‰ , and a calculated temperature of $\sim 74^{\circ}\text{C}$, albeit with high uncertainty (Table 1 and Figure 7c).

$\delta^{13}\text{C}$ and $\delta^{18}\text{O}$ values for Urdach samples range from -5 to $+1\text{‰}$ and from -11 to -4‰ , respectively (Figure 7a). Data cluster into two main groups: one with $\delta^{13}\text{C}$ values around 0‰ but showing a trend in which $\delta^{13}\text{C}$ decreases with decreasing $\delta^{18}\text{O}$ (group A); and the other, represented by only three samples, with lower values of $\delta^{13}\text{C}$ ($< -2\text{‰}$) and $\delta^{18}\text{O}$ close to -4‰ (group B). Two clumped isotope analyses were performed on one representative sample of each group. For the first (sample OFC-C3), values of 207°C and $\delta^{18}\text{O}_{\text{fluid}}$ of 11.9‰ were obtained, whereas for the second (sample OFC-C4), 229°C and $\delta^{18}\text{O}_{\text{fluid}}$ of 17.9‰ were found. Clerc et al. [2013] found values of $\delta^{13}\text{C}$ from -5 to $+1\text{‰}$ and $\delta^{18}\text{O}$ from -12.5 to -8.6‰ for Urdach ophtalcites, values that are consistent with our first group (group A).

The two analyzed Lherz ophtalcite samples show $\delta^{13}\text{C}$ and $\delta^{18}\text{O}$ values of -0.7 to -1.1‰ and -9.3 to -5.6‰ , respectively. Temperatures derived from clumped isotopes are relatively low, 32°C and 42°C , and $\delta^{18}\text{O}$ values for the fluid are -5.2‰ and -6.7‰ (Figures 7b and 7c). In the same type of ophtalcites from Lherz, Clerc et al. [2013] obtained values for $\delta^{13}\text{C}$ ranging from -1.6 to $+1\text{‰}$ and for $\delta^{18}\text{O}$ from -7.6 to -5.7‰ , which are also consistent with our measurements (Figure 7a).

Finally, also included in Figure 7a are the values for the Moncaup ophtalcite (sample MP84), in the Central Pyrenees, from Clerc et al. [2013], to highlight the similarity of their isotopic values to those of the Ziga breccia. It is worth noting that the Moncaup ultramafic body is capped by an extensional detachment with Jurassic marbles on top, and that slices of crystalline basement rocks and Keuper breccias are also observed along the complex contact zone [Lagabrielle et al., 2010].

7. Interpretation and Discussion

7.1. Ziga Ophicalcites

The isotopic signature of the calcite veins collected in one of the largest peridotite blocks outcropping in the Ziga *mélange* shows a vertical trend in the $\delta^{18}\text{O}$ - $\delta^{13}\text{C}$ plot, with relatively constant values of $\delta^{18}\text{O}$ around -4.5‰ , while the ophicalcite breccia shows slightly lower $\delta^{18}\text{O}$ values, between -7 and -6‰ . According to the classical assumption of a marine origin for the fluid ($\delta^{18}\text{O}_{\text{SMOW}} = 0\text{‰}$), the temperatures of precipitation would be $\sim 36^\circ\text{C}$ for the ophicalcite and $48\text{--}50^\circ\text{C}$ for the ophicalcite breccia [according to *Friedman and O'Neil, 1977*]. Assuming Cretaceous seawater with a $\delta^{18}\text{O}_{\text{SMOW}}$ of -1.2‰ [*Shackleton and Kennett, 1975*], temperatures calculated would be $\sim 29^\circ\text{C}$ and $41\text{--}43^\circ\text{C}$, respectively. The clumped isotopes in this case suggest that the calcite in the ophicalcite samples grew at even lower temperatures (Table 1) and precipitated from meteoric fluids, while the breccia records hotter but less well constrained temperatures: $49 \pm 37^\circ\text{C}$. Even considering that the Δ_{47} - T calibration may not be very accurate for the low- T range of the ophicalcite samples, it is clear that the resulting temperature is unexpectedly low. Although an analytical artifact or sample contamination cannot be completely discarded, the two ophicalcite samples show similar results with small standard errors (1.1 and 1.5°C) for 8 and 10 replicates. In any case, slightly hotter temperatures for these samples, such as those recorded for the breccia, would not significantly change our interpretation of the tectonic setting.

Potential sources of light carbon isotopic signatures could be: (i) magmatic CO_2 from the widespread Cretaceous magmatism in the Basque Cantabrian Region [*Rossy, 1988; Castaños et al., 2001*]. Although specific outcrops are lacking in the Marble Unit, this magmatism intruded into the Albian to Santonian materials from the Basque Arc [e.g., *Carracedo et al., 1999*]; (ii) oxidation of methane released during serpentinization [e.g., *Shanks et al., 1995*] or (iii) oxidation of organic matter in the sediments or soils [e.g., *Peter and Shanks, 1992; Eickmann et al., 2009*]. Meteoric fluids may wash the organic matter present in soils and/or the organic rich sediments of the late Albian terrigenous flysch (Mariako Gaina Formation) [*Bodego et al., 2015*].

Slightly negative $\delta^{13}\text{C}$ values are commonly associated with meteoric fluids at the surface, but to achieve the low values found in Ziga, the meteoric fluid might have interacted with oxidized organic matter contained in soils and vegetation [*Keith and Weber, 1964; Clerc et al., 2013*]. For example, *Swanson et al.* [2012] reported $\delta^{13}\text{C}$ values as low as -8‰ in carbonates precipitated from meteoric fluids in the Mormon Peak Detachment of the Basin and Range (Nevada), which they relate to oxidation of soil organic matter. *Quesnel et al.* [2013] obtained similar carbon isotopic signatures ($-16.7\text{‰} < \delta^{13}\text{C} < -8.5\text{‰}$) in magnesite veins in the New Caledonian peridotite massif. Based on the isotopic results and comparing them with several magnesite veins hosted by ultramafic rocks, they conclude that these ophicalcites were formed from meteoric waters with an organic carbon contribution either from surface soil or from a deep-seated source for those samples with $\delta^{13}\text{C}$ around -15‰ . They estimate temperatures of $38\text{--}77^\circ\text{C}$ based on the fractionation factor of magnesite and water.

$\delta^{13}\text{C}$ values similar to those of the Ziga ophicalcite breccia have been recorded by *Clerc et al.* [2013] for a microconglomerate and for micrite filling up veins and cavities in the altered and dislocated peridotite observed along the detachment zone capping the Moncaup peridotites. These authors interpret them as low-temperature ophicalcites with an influence of organic material, but they do not specify whether the formation was contemporaneous with the early Cretaceous exhumation stage or was the result of a later karstification and/or replacement of pre-existing ophicalcites. In any case, the Moncaup ophicalcites do not reflect seafloor exposure of an ultramafic basement, and accordingly, sedimentary breccias with ultramafic and crustal components are not observed.

Very low $\delta^{13}\text{C}$ values in carbonates could also be explained by a carbonation process driven by CO_2 uptake by hyperalkaline solutions derived from hydrating peridotite in surface conditions. In the Oman ophiolite, *Falk et al.* [2016] characterized recent peridotite-hosted travertines which gave values of $\delta^{13}\text{C}$ as low as -25‰ with $\delta^{18}\text{O}$ of -20 to 0‰ and high Δ_{47} values ($0.675\text{--}0.883\text{‰}$), the $\delta^{18}\text{O}$ for the formational fluid ranging from -1.5 to 2.5‰ and spring water temperature ranging between 17.6 and 38.4°C . *Streit et al.* [2012] also studying the Oman ophiolite, estimated a range of temperatures for the carbonate samples between 15 and 50°C and detected oxygen isotopic signatures similar to those of the groundwater and alkaline spring waters in peridotite catchments. However, calling for this type of process to explain the Ziga veins implies that they were formed once the wrenched peridotite blocks were already at the surface,

included in the *mélange*, and as we mention before, we could not find evidence of ophicalcite-like veins outside the peridotite blocks. Moreover, the volume of mapped peridotites in Ziga is not sufficiently significant ($<10 \text{ m}^3$), and typical travertine textures such as “surface films” at the surface of the springs or “bottom floc” as unconsolidated carbonate lining in the spring pools, as described by *Falk et al.* [2016] are not identified in the Ziga *mélange*.

As can be seen from petrography, CL and SEM images, all veins and veinlets are recrystallized (Figures 5c–5f) from a previous carbonate phase. Several authors have identified recrystallization of carbonates at low temperatures. For example, *Machel et al.* [1996], studying several phases of carbonate cementation and recrystallization in the Western Canada Sedimentary Basin, estimated recrystallization temperatures at 13–15°C [based on *O’Neil et al.*, 1969]. Very recent studies of clumped isotopes applied to the study of fluids in faults have also found temperatures as low as 13–24°C in carbonates precipitated from meteoric waters [*Swanson et al.*, 2012; *Bergman et al.*, 2013; *Sumner et al.*, 2015]. These studies have demonstrated that highly permeable zones, especially at the intersection of faults (as in this case the intersection between the Leiza and Pamplona faults) allow the rapid percolation of meteoric fluids and the precipitation of low-T carbonates before the fluid is heated at depth [*Bergman et al.*, 2013]. *Sumner et al.* [2015] even reported a carbonate precipitated at 19°C at $\sim 800 \text{ m}$ depth in a well, close to a fault that allowed rapid infiltration of meteoric waters.

Clumped isotope temperatures for the Ziga ophicalcites may point as well to a colder past climate. A climate shift in the Pyrenees occurred from the late Pliocene [e.g., *Babault et al.*, 2005] and *Fauquette et al.* [2007] estimated a mean annual temperature of 8–12°C in north-central Spain for the Mid-Pliocene based on pollen analysis. In any case, our data set lacks the necessary resolution to link recrystallization with specific past periods based on their average temperatures.

According to the above discussion, three hypotheses can be envisaged for the formation of the carbonate veins in Ziga: (i) they are typical ophicalcites formed at the seafloor due to complete mantle exhumation during the Cretaceous, but their isotopic composition changed due to cold meteoric fluids circulation that interacted with the organic matter present in soils and/or basin sediments, replacing the previous carbonate minerals; (ii) they are veins formed during the Late Cretaceous in serpentinized mantle rocks unroofed by the Leiza detachment but still covered by the Mesozoic sediments. Their isotopic composition must have changed for the same reasons explained in (i); and (iii) they are the postexhumation crystallization product of meteoric fluids that interacted with organic matter present in soils and sediments in different pulses. Since there is no single evidence of peridotite exposure to the seafloor (e.g., presence of sedimentary breccias with peridotite clasts, or veins with relict isotopic composition reflecting precipitation from seawater), we dismiss the first hypothesis. As the calcite veins seem to be concentrated inside the peridotite blocks within the *mélange*, we favor the second hypothesis. In this setting, the altered ultramafic rocks were progressively crunched in the Leiza detachment beneath the pre-rift cover and incorporated to the tectonic *mélange* developed in the Keuper evaporites. The presence of relicts of aragonite also makes the third hypothesis less plausible.

Precipitation of acicular aragonite could take place in a shallow marine environment [e.g., *Grotzinger and Reed*, 1983] or be related to warm waters with high salinity and high carbonate concentration [*Folk*, 1974]. Hence, aragonite may have crystallized in a first step during the extensional period, in a deep environment, with high salinity due to the presence of the Triassic salt above the detachment. Subsequently, during or after the tectonic inversion stage, meteoric fluids may have percolated downward, interacting with the organic matter-rich soils and/or sediments present in the area, producing the recrystallization of the previous carbonate mineralogy, resetting the $\delta^{18}\text{O}$ and the $\delta^{13}\text{C}$.

7.2. Marble Unit and Central Depression

Most of the samples belonging to the Marble Unit and the Central Depression, give values close to the original signature of Mesozoic marine limestones [*Keith and Weber*, 1964] (Figure 7a). Samples with lower $\delta^{18}\text{O}$ and $\delta^{13}\text{C}$ values are located in the eastern half of the Marble Unit, close to the Pamplona fault and/or related to intense tectonization. In fact, the samples with the strongest negative values are found in the marble block inside the *mélange* (MR1 and MR2), in two samples from the eastern most part of the Marble Unit, close to the Pamplona fault (MM16 and MM22a,b) and in the marble breccia collected in the Marble Unit (MM34, analysis of the matrix).

It is well-known that marbles can preserve their pre-metamorphic isotope signatures with only minor shifts in relation to devolatilization during prograde metamorphism [e.g., *Satish-Kumar*, 2001]. Trends of sympathetic decreases of $\delta^{18}\text{O}$ and $\delta^{13}\text{C}$ values can be caused by increasing volatilization (although this is generally not the dominant process, and would cause a curved shape in the depletion trend with an increasing slope towards low $\delta^{18}\text{O}$ values, which is not observed in our case), by variable temperature of equilibrium, or by infiltration of fluids in the later stages of metamorphic evolution or during the retrograde exhumation (meteoric fluids would cause a depletion in $\delta^{18}\text{O}$, whereas carbonic fluids would cause marked shifts in both $\delta^{18}\text{O}$ and $\delta^{13}\text{C}$ values) [e.g., *Valley*, 1986; *Satish-Kumar*, 2001].

The fact that most of the samples in the Marble Unit preserve the isotopic composition of the marine limestone protoliths, indicates that the metamorphism did not change the isotopic carbon and oxygen composition of these rocks in a significant way. Only those samples clearly associated with major tectonic structures, exhibit depleted $\delta^{18}\text{O}$ and $\delta^{13}\text{C}$, and therefore we argue that this depletion is caused by an isotopic exchange with fluids of different compositions, temperatures, and fluid-rock ratios. The occurrence of the most depleted marbles in proximal areas to the Pamplona fault may be due to more intense fluid circulation and/or higher temperatures of crystallization in the contact between the Leiza and Pamplona faults. The intersection of both faults may favor interaction of mantle-derived fluids with percolated meteoric fluids. The $\delta^{18}\text{O}$ composition of the formational fluid, assuming an open system, would indicate a slightly heavier composition than that of marine seawater, suggesting at least a partial contribution from more saline and/or magmatic fluids.

7.3. Urdach and Lherz Ophicalcites

For the Urdach samples, the linear trend of group A observed in the $\delta^{18}\text{O}$ - $\delta^{13}\text{C}$ diagram of Figure 7a probably indicates different degrees of fluid-rock interaction and an isotopic evolution and differentiation of the fluid in agreement with the consecutive formation of veins. $\delta^{13}\text{C}$ values cluster around 0‰, which is the typical isotope signature of seawater carbonates. The three samples in group B, with lower $\delta^{13}\text{C}$ and higher $\delta^{18}\text{O}$ values, correspond to a later family of calcite veins (Figures 3c and 7b). If the composition of the fluid from which the calcite precipitated was that of seawater with $\delta^{18}\text{O}_{\text{SMOW}} = 0‰$, then the temperatures of precipitation according to the calcite-water fractionation factor of *Friedman and O'Neil* [1977] would be ~51–79°C for group A and 34°C for group B. Considering Cretaceous seawater with a $\delta^{18}\text{O}_{\text{SMOW}}$ of $-1.2‰$ [*Shackleton and Kennett*, 1975], temperatures estimated would be between 44 and 70°C for group A and 28°C for group B. Clumped isotopes data, however, point to much higher temperatures for the final crystallization event in both groups (~200–230°C). Considering that the mantle rocks displaying these ophicalcites were exhumed to the seafloor in the Albian-Cenomanian, those temperatures could only have been reached either before total exhumation, or by diagenesis after the extensional exhumation to the seafloor and before the tectonic inversion, when the ophicalcites were buried by the Late Cretaceous stratigraphic column. It is worth noting that two measurements of Raman Spectroscopy in the Cenomanian sediments immediately adjacent to the peridotite body, yielded virtually identical temperatures: 215 and 233°C [*Clerc*, 2013]. This observation strongly suggests that the ophicalcites were recrystallized during the Upper Cretaceous, under the same sedimentary burial that affected the overlying Cenomanian sediments. The Cretaceous stratigraphic column in the Mail Arrouy basin plus some influence of hydrothermal fluid circulation can easily explain those temperatures at the base of the basin. In this tectonic scenario, significant fluid circulation (either basinal or metamorphic fluids) is expected along the “damage zone” represented by the extensional detachment that exhumed the mantle and was covered by the Late Cretaceous sediments. In such an open-system environment, the clumped isotope results suggest that the composition of the parent fluid was a saline or metamorphic type of fluid rather than seawater.

This is not particularly surprising, considering that the extensional detachment responsible for the exhumation of the Urdach peridotites was to a great extent initiated in a decoupling horizon represented by a thick Triassic evaporite layer, widely accumulated at the base of the Mauléon basin [*Jammes et al.*, 2009, 2010; *Corre et al.*, 2016]. According to these authors, the late Aptian to early Albian basin was flooded directly by the exhumed mantle and lower crustal rocks. Since there is clear evidence of submarine sedimentary reworking of the exhumed mantle, we can expect the formation of “typical” ophicalcites at or very near the seafloor. But unless concentrated in spots of high hydrothermal activity (Mid-Atlantic Ridge hydrothermal fields) [e.g., *Andreani et al.*, 2014], “typical” ophicalcites formed over exposures of mantle rocks directly at the seafloor are expected to reflect signatures of colder and less saline fluids (i.e., typical marine waters),

such as those from the Iberian margin [Agrinier *et al.*, 1988; Schwarzenbach *et al.*, 2013; Klein *et al.*, 2015] or from the Mid-Atlantic Ridge [Kelley *et al.*, 2005]. Since those signatures are not observed in our samples, we consider that the primary opicalcites were buried by the Upper Cretaceous sediments and recrystallized under a hot geothermal gradient. The fluids responsible for the recrystallization were most probably marine waters, infiltrated through faults, circulating through the Upper Cretaceous sediments, heated up progressively and becoming more saline by interaction with the Keuper evaporites that remained as tectonic lenses directly above the extensional detachment, before finally reaching the serpentinized mantle. According to this scenario, the episode of vein recrystallization recorded by the clumped isotopes would be produced in a relatively deep and warm environment at the base of the basin, rather than at the seafloor.

The opicalcites cropping out in Lherz have $\delta^{13}\text{C}$ and $\delta^{18}\text{O}$ -values only slightly different from those of Urdach. Relying on the classical assumption of marine water composition for the fluid ($\delta^{18}\text{O}_{\text{SMOW}}$ in the range -1.2 to 0‰), the temperatures of precipitation would be in the range of $\sim 35\text{--}66^\circ\text{C}$ according to the fractionation factor of Friedman and O'Neil [1977]. Interestingly, in this case, the clumped isotope thermometer reports similar or even slightly lower temperatures: between 32 and 42°C . Therefore, in spite of the similarity between the Lherz and Urdach opicalcites in terms of $\delta^{13}\text{C}$ and $\delta^{18}\text{O}$ values, the clumped isotope data suggest that the Lherz opicalcites were formed at much lower temperatures and from fluids of meteoric origin. All these data point to a superficial environment of formation, where the calcite precipitated either in a post-tectonic stage at near ambient temperatures close to the surface or under shallow diagenetic conditions. It should be noted that we only analyzed calcite veins from one of the four types of breccias described by Lagabrielle and Bodinier [2008] in the Lherz body, namely the sedimentary breccias of Type 4. Previous $\delta^{18}\text{O}$ and $\delta^{13}\text{C}$ isotopic determinations by Clerc *et al.* [2013] show that the signature of these veins are not significantly different from those of the other types around the main peridotite body in Lherz, and they define the whole dataset as sedimentary opicalcites, formed in association with the bordering breccias. The opicalcites have slightly high $\delta^{18}\text{O}$ when compared to the western Pyrenean opicalcites, which according to Clerc *et al.* [2013], would reflect a warmer temperature and may be related to sedimentary fluids in an endorheic basin. Due to the meteoric nature inferred for the fluid and the temperatures we find for these opicalcites (at least for the veins in the Type 4 breccias), we find this explanation plausible, although post-tectonic recrystallization at near surface conditions (1–2 km depth) is also highly probable.

7.4. Evolutionary Setting for the Eastern Basque-Cantabrian Basin

A conceptual tectonic model for the late Albian is presented in Figure 8. Related to the opening of the Bay of Biscay, progressive crustal thinning took place in the western-central Pyrenees and eastern Basque-Cantabrian Basin and led to local mantle unroofing to the base of the Cretaceous basins, under the pre-rift sedimentary cover [e.g., Lagabrielle *et al.*, 2010; Clerc and Lagabrielle, 2014; Teixell *et al.*, 2016]. In the area studied, that exhumation was facilitated by the Leiza detachment system that put both the mantle and deep crust into contact with the Keuper-facies salts at the base of the basin. During the extensional uplift of the peridotite body, it was progressively serpentinized as the temperature was decreasing. Antigorite, observed in our peridotite samples and commonly found in higher temperature settings such as mantle wedges above subduction planes, is very uncommon in extensional settings [e.g., Guillot *et al.*, 2015]. However, it has been previously described in the western Pyrenees, in the Chaînons Béarnais (Sarailié), in locations with considerable deformation [Ferreira *et al.*, 2014]. The local existence of this variety may probably be due to the emplacement of the mantle underneath the detachment fault in relation to a shear zone [Evans, 2004].

The mantle uplift induced a thermal anomaly in the basin that gave rise to the metamorphism of the Marble Unit, the widespread occurrence of hydrothermalism in the Central Depression [Iriarte, 2004], and a significant remagnetization event. Larrasoña *et al.* [2003b] describe a remagnetization event in the red beds of the Triassic Buntsandstein facies in the Cinco Villas and Alduides massifs at $300\text{--}650^\circ\text{C}$, which they link to fluid circulation during the Cretaceous (pre-Turonian). Hydrothermalism has been identified in the Albian to Turonian materials of the Central Depression, where fluid inclusions in fracture-sealing cement and authigenic quartz yield temperatures of less than 185°C and high salinities [Iriarte *et al.*, 2011].

In the reconstruction proposed in Figure 8, an evaporitic/tectonic *mélange* is formed at the detachment, in the shear zone. This *mélange* should have developed in the salts of the Keuper facies. It cannot be discarded that part of the pre-rift carbonates belonging to the Marble Unit also behaved as a ductile layer at the

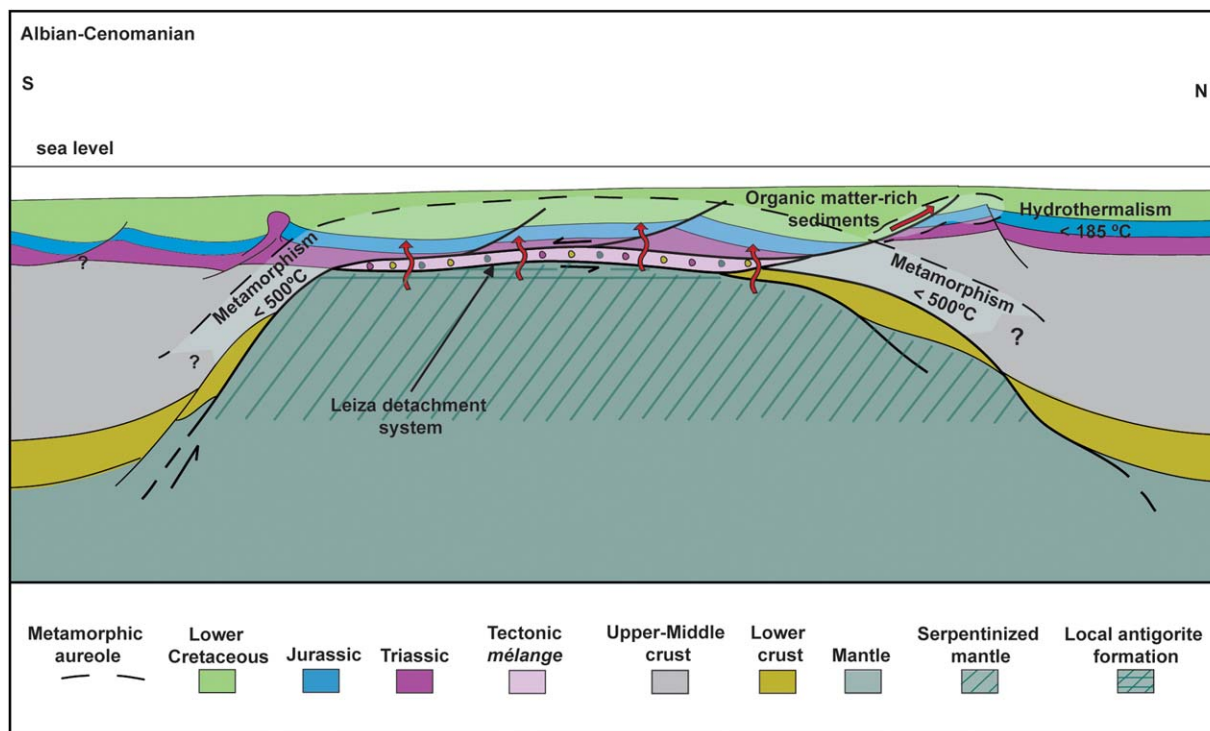


Figure 8. Conceptual tectonic model of hyperextended crust and mantle unroofing during Albian-Cenomanian times in the eastern border of the Basque-Cantabrian Basin. The exhumation is promoted by the Leiza detachment system, which represents a preferential path for the fluids. No evidence for a complete underwater exhumation of the mantle was found for this basin.

maximum temperature of the metamorphism as described by *Lagabrielle et al.* [2016] for the Aulus basin, *Corre et al.* [2016] for the Mauléon basin and *Vauchez et al.* [2013] for the Agly massif. During the extensional period, the detachment was able to tear pieces of the mantle and lower crust as well as pieces of Paleozoic and Triassic materials which are mapped all along the inverted Leiza fault trace [*Mendia and Gil Iburguchi*, 1991].

During the unroofing of the mantle, serpentinization took place as soon as the temperature was low enough ($< \sim 500^{\circ}\text{C}$) and the fluids percolating from the surface reached the peridotites. Infiltration of fluids interacting with the late Albian organic matter-rich sediments, may have promoted the carbonation process in the peridotites under the Mesozoic sedimentary cover. However, we do not keep the isotopic record of these early and relatively hot veins in our dataset. During the alpine inversion of the basin, the Leiza fault acted as a thrust fault uplifting all the Marble Unit over the Central Depression, and carrying slices of basement and Triassic materials to the surface. Since the Ziga *mélange* was mainly composed of plastic evaporitic materials, it was forced out through the most favorable path, which was the junction between the Leiza and Pamplona faults. Although several diapirs in surrounding basins began to extrude during the Cretaceous [e.g., *Iriarte*, 2004], a mid-Eocene apatite-fission-track age in a granulite from the *mélange*, indicates that the Ziga *mélange* was extruded during the alpine orogeny (*DeFelipe et al.*, in preparation). We postulate that the last and low-temperature recrystallization event responsible for the isotopic compositions found in our calcite veins samples, occurred with the peridotite blocks close to or almost at the surface in a meteoric water environment with the contribution of sedimentary or soil organic carbon.

8. Conclusions

Carbonation in peridotites is a complex process that can take place under many different conditions and is not restricted to seawater alteration of serpentinized peridotites. It deserves further investigation on a case by case basis in order to understand the tectonic framework in which they were formed. The combination of petrographic and mineralogical description, stable and clumped isotope analysis in carbonate rocks, allows mineral characterization and determination of temperatures of recrystallization together with

possible oxygen isotope signature of the fluid. Combination of these techniques and fieldwork constraints in three different types of peridotite-hosted calcite veins yielded three different results: (i) recrystallization from cold meteoric fluids with light carbon derived from organic matter and affecting a primary carbonate phase that can hardly be related to typical ophicalcites formed at the seafloor in the Ziga outcrops; (ii) characterization of ophicalcites formed by mantle exhumation to the seafloor and later recrystallized in a hot and saline environment (Urdach) and (iii) ophicalcites recrystallized from meteoric fluids at relatively low temperature, without significant input from organic matter (Lherz). For the calcite veins in the Ziga peridotite, petrographic and geochemical evidence reflects a previous aragonite phase that was recrystallized by meteoric waters that reacted with organic matter in soils and sediments. The primary carbonate phase may have been formed most probably during the Cretaceous after mantle unroofing to the base of the sedimentary pile of the basin, although a postexhumation formation cannot be completely discarded. Carbonates from the Marble Unit and Central Depression predominantly reflect the original marine signature of the parent limestones (with some depletion for the oxygen signature). However, getting close to the Pamplona fault, both $\delta^{13}\text{C}$ and $\delta^{18}\text{O}$ values decrease progressively reaching the lowest values in the marble of the Ziga *mélange* (MR1 sample), which could be interpreted in terms of a more intense fluid circulation around the junction of both faults.

Urdach ophicalcites were probably formed at relatively low temperatures when the mantle was exposed at the sea bottom in the Albian-Cenomanian, although that event was not identified in our dataset. Recrystallization might well have taken place during the Late Cretaceous, under a sedimentary cover and hydrothermal fluid circulation that may favor general temperatures at the base of the sedimentary pile of 200–230°C (recorded by both the ophicalcites and the Cenomanian sediments directly above). Finally, the recrystallization event found in the Lherz ophicalcites took place relatively near the surface, from meteoric fluids at temperatures of 32–42°C, either under very shallow diagenetic conditions or in a post-tectonic stage.

The tectonic framework proposed for the eastern border of the Basque-Cantabrian Basin is that of a hyperextended basin where the mantle and lower crust were exhumed at the base of the sedimentary pile of the Cretaceous basin during the stage of maximum extension in the late Albian. The main extensional detachment developed partially along the weak layer represented by the Triassic evaporites, and wrenched fragments from the mantle and the lower crust were embedded into these plastic materials forming the Ziga *mélange*. According to their way of emplacement, these peridotites would fall into the “tectonic type” (T type) of *Lagabrielle et al.* [2010], in contrast to the “sedimented type” (S type) of the Lherz peridotites. The Mesozoic sediments located on top of the detachment experienced HT-LP metamorphism at this time, forming the Marble Unit. During the alpine orogeny, the Leiza fault was inverted and this movement was able to remobilize the plastic Keuper-facies evaporites with embedded fragments of deep-seated rocks, taking them to the surface. This *mélange* rose through the most favorable and mechanical weak zone, the junction between the Leiza and Pamplona faults, which was also a favorable conduct for fluid flow. Cold meteoric fluids infiltrated along this conduct, producing the recrystallization of carbonates at temperatures lower than 49°C.

The results presented, especially for the Urdach ophicalcites, warn us of the risk of assuming the $\delta^{18}\text{O}$ value for the fluid when calculating the precipitation temperatures from the value of $\delta^{18}\text{O}$ in carbonates. Clumped isotope thermometry avoids this uncertainty by directly retrieving a measure of the fluid isotopic composition. For these reasons, the combination of these approaches is a very useful tool for understanding carbonation processes in hyperextended settings such as those investigated in this study. However, a more numerous and systematic sampling in different generation of veins would be necessary in each locality to achieve a more complete picture of the detailed succession of events in each particular case.

References

- Agrinier, P., C. Mével, and J. Girardeau (1988), Hydrothermal alteration of the peridotites cored at the ocean/continental boundary of the Iberian Margin: Petrologic and stable isotope evidence, *Proc. Ocean Drill. Program Sci. Results*, 103, 225–234.
- Albarède, F., and A. Michard-Vitrac (1978), Age and significance of the North Pyrenean metamorphism, *Earth Planet. Sci. Lett.*, 40(3), 327–332.
- Álvarez, M., et al. (1994), *Mapa Geológico de la Península Ibérica, Baleares y Canarias*, Inst. Geol. y Minero de España (IGME), Spain.
- Andreani, M., J. Escartin, A. Delacour, B. Ildefonse, M. Godard, J. Dymont, A. E. Fallick, and Y. Fouquet (2014), Tectonic structure, lithology, and hydrothermal signature of the Rainbow massif (Mid-Atlantic Ridge 36°14'N), *Geochem. Geophys. Geosyst.*, 15, 3543–3571, doi: 10.1002/2014GC005269.
- Babault, J., J. Van Den Driessche, S. Bonnet, S. Castelltort, and A. Crave (2005), Origin of the highly elevated Pyrenean peneplain, *Tectonics*, 24, TC2010, doi:10.1029/2004TC001697.

Acknowledgments

We thank the PhD financial support for IDF, given by the University of Oviedo-Banco Santander, Government of the Principality of Asturias and the FPU grant of the Spanish Ministry of Education, Culture and Sport. This is a contribution of the Ministry of Economy and Competitiveness Project MISTERIOS (CGL2013-48601-C2-2-R), the Consolider-Ingenio 2010 Project TOPO-IBERIA (CSD2006-00041), and the ESF TopoEurope Project PYRTEC (SV-PA-10-03-IP2-PYRTEC). We thank Heather Stoll and the staff of the stable isotope laboratories of the Universities of Oviedo and Barcelona and ETH-Zürich for their support. We want to give special thanks to Stefano Bernasconi for interesting discussions and laboratory assistance. Yves Lagabrielle and Serge Fourcade are thanked for their very useful and constructive reviews. Email address for correspondence: defelipe@geol.uniovi.es.

- Bach, W., C. J. Garrido, H. Paulick, J. Harvey, and M. Rosner (2004), Seawater-peridotite interactions: First insights from ODP Leg 209, MAR 15°N, *Geochem. Geophys. Geosyst.*, 5, Q09F26, doi:10.1029/2004GC000744.
- Barbieri, M., U. Masi, and L. Tolomeo (1979), Stable isotope evidence for a marine origin of opicalcites from the North-Central Apennines (Italy), *Mar. Geol.*, 30, 193–204.
- Bergman, S. C., K. W. Huntington, and J. G. Crider (2013), Tracing paleofluid sources using clumped isotope thermometry of diagenetic cements along the Moab Fault, Utah, *Am. J. Sci.*, 313, 1–26, doi:10.2475/04.2013.00.
- Bernoulli, D., and H. Weissert (1985), Sedimentary fabrics in Alpine opicalcites, South Pennine Arosa zone, Switzerland, *Geology*, 13, 755–758, doi:10.1130/0091-7613(1985)13<755.
- Bodego, A., E. Iriarte, L. M. Agirrezabala, J. García-Mondéjar, and M. A. López-Horgue (2015), Synextensional mid-Cretaceous stratigraphic architecture of the eastern Basque–Cantabrian basin margin (western Pyrenees), *Cretaceous Res.*, 55, 229–261, doi:10.1016/j.cretres.2015.01.006.
- Bonney, T. G. (1879), Notes on some Ligurian and Tuscan serpentinites, *Geol. Mag.*, 6(2), 362–371.
- Brongniart, A. (1813), Essai d'une classification minéralogique des roches mélangées, *J. des Mines*, 199, 48.
- Canérot, J., and F. Delavaux (1986), Tectonic and sedimentation on the north Iberian margin, Chainons Béarnais south Pyrenean zone (Pyrenees basco-béarnaises): New data about the signification of the Iherzolites in the Sarailé area, *C. R. Acad. Sci. Ser. II*, 302(15), 951–956.
- Canérot, J., C. Majesté-Menjoules, and Y. Ternet (2004), Nouvelle interprétation structurale de la "faille Nord-Pyrénéenne" en vallée d'Aspe (Pyrénées-Atlantiques). Remise en question d'un plutonisme ophitique danien dans le secteur de Bedous, *C. R. Geosci.*, 336(2), 135–142, doi:10.1016/j.crte.2003.11.004.
- Carbayo, A., L. León, and L. Villalobos (1977), *Mapa Geológico de España E, 1:50.000, Hoja 115, Gulina*, Inst. Geol. y Minero de España (IGME), Spain.
- Carracedo, M., F. J. Larrea, and A. Alonso (1999), Estructura y organización de las coladas submarinas: Características de las lavas almohadilladas de edad Cretácica que afloran en la Cordillera Vasco-Cantábrica, *Estud. Geol.*, 55, 209–222.
- Castañares, L. M., S. Robles, D. Gimeno, and J. C. Vicente Bravo (2001), The submarine volcanic system of the Errigoiti formation (Albian-Santonian of the Basque-Cantabrian Basin, Northern Spain): Stratigraphic framework, facies, y sequences, *J. Sediment. Res.*, 71, 318–333.
- Casteras, M. (1970), *Carte géol. France (1/50 000), feuille Oloron-Sainte-Marie (XV-46), notice*, 19 pp. (1971), BRGM éd., Orléans, France.
- Choukroune, P. (1976), Structure et évolution tectonique de la zone nord-pyrénéenne: Analyse de la déformation dans une portion de chaîne à schistosité verticale, *Mém. Soc. Géol. Fr.*, 127, 1–116.
- Clerc, C. (2013), Évolution du domaine Nord-Pyrénéen au Crétacé. Amincissement crustal extreme et thermicité élevée: Un analogue pour les marges passives, PhD thesis, Univ. Paris 6, Paris.
- Clerc, C., and Y. Lagabriele (2014), Thermal control on the modes of crustal thinning leading to mantle exhumation: Insights from the Cretaceous Pyrenean hot paleomargins, *Tectonics*, 33, 1340–1359, doi:10.1002/2013TC003471.
- Clerc, C., P. Boulvais, Y. Lagabriele, and M. de Saint Blanquat (2013), Opicalcites from the northern Pyrenean belt: A field, petrographic and stable isotope study, *Int. J. Earth Sci.*, 103(1), 141–163, doi:10.1007/s00531-013-0927-z.
- Clerc, C., A. Lahfid, P. Monié, Y. Lagabriele, C. Chopin, M. Poujol, P. Boulvais, J.-C. Ringenbach, E. Masini, and M. de St Blanquat (2015), High-temperature metamorphism during extreme thinning of the continental crust: A reappraisal of the north Pyrenean paleo-passive margin, *Solid Earth Discuss.*, 7(1), 797–857, doi:10.5194/sed-7-797-2015
- Corre, B., Y. Lagabriele, P. Labaume, S. Fourcade, C. Clerc, and M. Ballèvre (2016), Deformation associated with mantle exhumation in a distal, hot passive margin environment: New constraints from the Sarailé Massif (Chainons Béarnais, North-Pyrenean Zone), *C. R. Geosci.*, 348(3–4), 279–289, doi:10.1016/j.crte.2015.11.007.
- Debroas, E.-J., J. Canérot, and M. Bilotte (2010), Les Brèches d'Urdach, témoins de l'exhumation du manteau pyrénéen dans un escarpement de faille vracconien-cénomanién inférieur (zone nord-pyrénéenne, Pyrénées-Atlantiques, France), *Géol. France*, 2, 53–64.
- DeFelipe, I., D. Pedreira, J. A. Pulgar, E. Iriarte, and M. Mendia (2012a), Petrography, mineralogy and stable isotopes in opicalcites in the surroundings of Ziga (Basque-Cantabrian Region), in *VIII Congreso Geológico de España, Oviedo. Geo-Temas*, vol. 13, pp. 505–508.
- DeFelipe, I., D. Pedreira, J. A. Pulgar, E. Iriarte, and M. Mendia (2012b), Petrography and C and O stable isotope composition of opicalcites in the Western Pyrenees/Eastern Cantabrian Mountains: Geodynamic implications, *Geophys. Res. Abstr.*, 14, EGU2012–12448.
- Del Valle, J., et al. (1973), *Mapa Geológico de España E, 1:50.000, Hoja 90, Sumbilla*, Inst. Geol. y Minero de España (IGME), Spain.
- Duée, G., Y. Lagabriele, A. Coutelle, and A. Fortané (1984), Les Iherzolites associés aux chainons béarnais (Pyrénées Occidentales): Mise à l'affleurement anté-Dogger et resédimentation albo-cénomanién, *C. R. Acad. Sci. Paris Ser. II*, 299, 1205–1209.
- Eickmann, B., W. Bach, and J. Peckmann (2009), Authigenesis of carbonate minerals in modern and Devonian Ocean-Floor hard rocks, *J. Geol.*, 117(3), 307–323, doi:10.1086/597362.
- Eiler, J. M. (2007), "Clumped-isotope" geochemistry—The study of naturally-occurring, multiply-substituted isotopologues, *Earth Planet. Sci. Lett.*, 262(3–4), 309–327, doi:10.1016/j.epsl.2007.08.020.
- Evans, B. W. (2004), The serpentinite multisystem revisited: Chrysotile is metastable, *Int. Geol. Rev.*, 46(6), 479–506, doi:10.2747/0020-6814.46.6.479.
- Fabriès, J., J.-P. Lorand, and J.-L. Bodinier (1998), Petrogenetic evolution of orogenic Iherzolite massifs in the central and western Pyrenees, *Tectonophysics*, 292, 145–467.
- Falk, E. S., W. Guo, A. N. Paukert, J. M. Matter, E. M. Mervine, and P. B. Kelemen (2016), Controls on the stable isotope compositions of travertine from hyperalkaline springs in Oman: Insights from clumped isotope measurements, *Geochim. Cosmochim. Acta*, 192, 1–28, doi:10.1016/j.gca.2016.06.026.
- Fauquette, S., et al. (2007), Latitudinal climatic gradients in the Western European and Mediterranean regions from the Mid-Miocene (c. 15 Ma) to the Mid-Pliocene (c. 3.5 Ma) as quantified from pollen data, in *Deep-Time Perspectives on Climate Change: Marrying the Signal from Computer Models and Biological Proxies, Micropalaeontol. Soc.*, edited by M. Williams et al., pp. 481–502, Geol. Soc., London.
- Ferreira, N., A. Delacour, M. De Saint Blanquat, P. Boulvais, M. Benoit, and Y. Lagabriele (2014), Conditions of formation of serpentinites in Pyrenees and new constraints on the model of exhumation of mantle peridotites, 24^{ème} Réunion des sciences de la Terre, Oct. 2014, Pau, France. Livre des résumés, pp. 229, 24.
- Folk, R. L. (1974), The natural history of crystalline calcium carbonate: Effect of magnesium content and salinity, *J. Sediment. Petrol.*, 44, 40–53.
- Fortané, A., G. Duée, Y. Lagabriele, and A. Coutelle (1986), Iherzolites and the Western "Chainons Béarnais" (French Pyrenees): Structural and paleogeographical pattern, *Tectonophysics*, 129(1), 81–98.
- Friedman, I., and J. R. O'Neil (1977), Compilation of stable isotope fractionation factors of geochemical interest, in *Data Geochem*, 6th ed., *Geol. Surv. Prof Pap 440K*, Technical Editor Michael Fleischer. United States Government Printing Office, Wash.
- Früh-Green, G. L., H. Weissert, and D. Bernoulli (1990), A multiple fluid history recorded in Alpine ophiolites, *J. Geol. Soc.*, 147(6), 959–970, doi:10.1144/gsjgs.147.6.0959

- Gabaldón, V., J. C. Fernández, A. O. Davó, J. R. Merino, J. S. Sedó, and L. V. Vilches (1983), *Mapa Geológico de España E, 1:50.000, Hoja 89, Tolosa*, Inst. Geol. y Minero de España (IGME), Spain.
- Gabaldón, V., J. R. Merino, A. O. Davó, L. V. Vilches, L. L. González, and A. C. Olivares (1984), *Mapa Geológico de España E, 1:50.000, Hoja 114, Alsasua*, Inst. Geol. y Minero de España (IGME), Spain.
- Ghosh, P., J. Adkins, H. Affek, B. Balta, W. Guo, E. A. Schauble, D. Schrag, and J. M. Eiler (2006), ^{13}C - ^{18}O bonds in carbonate minerals: A new kind of paleothermometer, *Geochim. Cosmochim. Acta*, *70*(6), 1439–1456, doi:10.1016/j.gca.2005.11.014.
- Golberg, J.-M., and A. F. Leyreloup (1990), High temperature-low pressure Cretaceous metamorphism related to crustal thinning (Eastern North Pyrenean Zone, France), *Contrib. Mineral. Petrol.*, *104*(2), 194–207, doi:10.1007/BF00306443
- Grauel, A. (2012), Calibration of the “clumped isotope” thermometer on foraminifera and its application to high-resolution climate reconstruction of the past 2500yr in the Gulf of Taranto (Eastern Mediterranean Sea), PhD Thesis, ETH Zurich, 181 pp.
- Grotzinger, J. P., and J. F. Reed (1983), Evidence for primary aragonite precipitation, lower Proterozoic (1.9 Ga) Rocknest dolomit, Wopimay Orogen, northwest Canada, *Geology*, *11*, 710–713.
- Guillot, S., S. Schwartz, B. Reynard, P. Agard, and C. Prigent (2015), Tectonic significance of serpentinites, *Tectonophysics*, *646*, 1–19, doi:10.1016/j.tecto.2015.01.020.
- Hall, C. A., and J. A. Johnson (1986), Apparent western termination of the North Pyrenean fault and tectonostratigraphic units of the western north Pyrenees, France and Spain, *Tectonics*, *5*, 607–627.
- Henkes, G. A., B. H. Passey, E. L. Grossman, B. J. Shenton, A. Pérez-Huerta, and T. E. Yancey (2014), Temperature limits for preservation of primary calcite clumped isotope paleotemperatures, *Geochim. Cosmochim. Acta*, *139*, 362–382.
- Huntington, K. W., D. A. Budd, B. P. Wernicke, and J. M. Eiler (2011), Use of clumped-isotope thermometry to constrain the crystallization temperature of diagenetic calcite, *J. Sediment. Res.*, *81*(9), 656–669, doi:10.2110/jsr.2011.51.
- Iriarte, E. (2004), La Depresión Intermedia entre Leizta y Elizondo (Pirineo occidental): Estratigrafía y relaciones tectónica-sedimentación durante el Cretácico, unpublished PhD thesis, 310 pp., Univ. País Vasco Fac. Ciencia y Tecnología, Leioa, Spain.
- Iriarte, E., A. López-Horgue, A. Aramburu, A. Bodego, A. Cerani, and J. García-Mondéjar (2011), Synsedimentary cretaceous hydrothermalism in the Leizta fault (Basque-Cantabrian Basin, western Pyrenees), Abstract Volume 23ème Réunion des Sciences de la Terre, Bordeaux, 25–29 October 2010, pp. 109–110, ISBN: 2-85363-096-X.
- Jammes, S., G. Manatschal, L. Lavier, and E. Masini (2009), Tectonosedimentary evolution related to extreme crustal thinning ahead of a propagating ocean: Example of the western Pyrenees, *Tectonics*, *28*, TC4012, doi:10.1029/2008TC002406.
- Jammes, S., C. Tiberi, and G. Manatschal (2010), 3D architecture of a complex transcurrent rift system: The example of the Bay of Biscay–Western Pyrenees, *Tectonophysics*, *489*(1–4), 210–226, doi:10.1016/j.tecto.2010.04.023.
- Keith, M. L., and J. N. Weber (1964), Carbon and oxygen isotopic composition of selected limestones and fossils, *Geochim. Cosmochim. Acta*, *28*, 1787–1816.
- Kelemen, P. B., and J. M. Matter (2008), In situ carbonation of peridotite for CO₂ storage, *Proc. Nat. Acad. Sci. U. S. A.*, *105*, 17,295–17,300.
- Kelley, D. S., et al. (2005), A serpentinite-hosted ecosystem: The lost city hydrothermal field, *Science*, *307*, 1428–1434, doi:10.1126/science.1102556.
- Klein, F., S. E. Humphris, W. Guo, F. Schubotz, E. M. Schwarzenbach, and W. D. Orsi (2015), Fluid mixing and the deep biosphere of a fossil Lost City-type hydrothermal system at the Iberia Margin, *Proc. Nat. Acad. Sci. U. S. A.*, *112*(39), 12,036–12,041, doi:10.1073/pnas.1504674112/-DCSupplemental.www.pnas.org/cgi/doi/10.1073/pnas.1504674112.
- Lagabrielle, Y., and J.-L. Bodinier (2008), Submarine reworking of exhumed subcontinental mantle rocks: Field evidence from the Lherz peridotites, French Pyrenees, *Terra Nov.*, *20*(1), 11–21, doi:10.1111/j.1365-3121.2007.00781.x.
- Lagabrielle, Y., P. Labaume, and M. de Saint Blanquat (2010), Mantle exhumation, crustal denudation, and gravity tectonics during Cretaceous rifting in the Pyrenean realm (SW Europe): Insights from the geological setting of the Lherzolite bodies, *Tectonics*, *29*, TC4012, doi:10.1029/2009TC002588.
- Lagabrielle, Y., C. Clerc, A. Vauchez, A. Lahfid, P. Labaume, B. Azambre, S. Fourcade, and J. M. Dautria (2016), Very high geothermal gradient during mantle exhumation recorded in mylonitic marbles and carbonate breccias from a Mesozoic Pyrenean palaeomargin (Lherz area, North Pyrenean Zone, France), *C. R. Geosci.*, *348*(3–4), 290–300, doi:10.1016/j.crte.2015.11.004.
- Lamare, P. (1936), Recherches géologiques dans le Pyrénées basques d'Espagne, *Mém. Soc. Géol. France, nouv. Sér.*, *II-27*, 462.
- Larrasoana, J. C., J. M. Parés, J. del Valle, and H. Millán (2003a), Triassic paleomagnetism from the Western Pyrenees revisited: Implications for the Iberian-Eurasian Mesozoic plate boundary, *Tectonophysics*, *362*(1–4), 161–182, doi:10.1016/S0040-1951(02)00636-4.
- Larrasoana, J. C., J. M. Parés, H. Millán, J. del Valle, and E. L. Pueyo (2003b), Paleomagnetic, structural, and stratigraphic constraints on transverse fault kinematics during basin inversion: The Pamplona Fault (Pyrenees, north Spain), *Tectonics*, *22*(6), 1071, doi:10.1029/2002TC001446.
- Lavoie, D. (1997), Hydrothermal vent bacterial community in Ordovician ophalcalcite, southern Quebec Appalachians, *J. Sediment. Res.*, *67*(1), 47–53.
- Lemoine, M., P. Tricart, and G. Boillot (1987), Ultramafic and gabbroic ocean floor of the Ligurian Tethys (Alps, Corsica, Apennines): In search of a genetic model, *Geology*, *15*, 622–625, doi:10.1130/0091-7613(1987)15<622.
- Llanos, H. J. (1983), *Estudio geológico del borde sur del macizo de Cinco Villas transversal Huici-Leiza (Navarra)*, Univ. País Vasco, UPV, EHU. 1980. Cuadernos de Sección. Ciencias Naturales. ISBN 84-7086-120-9. pp. 75–116.
- Lloyd, S. J., F. A. Corsetti, J. M. Eiler, and A. K. Tripathi (2012), Determining the diagenetic conditions of concretion formation: Assessing temperatures and pore waters using clumped isotopes, *J. Sediment. Res.*, *82*(12), 1006–1016, doi:10.2110/jsr.2012.85.
- Machel, H. G., P. A. Cavell, and K. S. Patey (1996), Isotopic evidence for carbonate cementation and recrystallization, and for tectonic expulsion of fluids into the Western Canada Sedimentary Basin, *Geol. Soc. Am. Bull.*, *108*, 1108–1119.
- Martínez-Torres, L. M. (2008), El Manto de los Mármoles (Pirineo Occidental): Geología estructural y evolución geodinámica, PhD thesis 1989, 294 pp., Univ. País Vasco, Bizkaia, Spain.
- Mathey, B., M. Floquet, and L. M. Martínez-Torres (1999), The Leiza palaeo-fault: Role and importance in the Upper Cretaceous sedimentation and palaeogeography of the Basque Pyrenees (Spain), *C. R. Acad. Sci. Ser. IIA*, *328*(6), 393–399, doi:10.1016/S1251-8050(99)80105-0.
- Mattauer, M. (1968), Les traits structuraux essentiels de la chaîne Pyrénéenne, *Rev. Geogr. Phys. Geol. Dyn.*, *2*, 3–12.
- McCrea, J. M. (1950), On the isotopic chemistry of carbonates and a paleotemperature scale, *J. Chem. Phys.*, *18*, 849–857.
- Mendia, M., and J. I. Gil Ibarguchi (1991), High-grade metamorphic rocks and peridotites along the Leiza Fault (Western Pyrenees, Spain), *Geol. Rund.*, *80*(1), 93–107.
- Mével, C. (2003), Serpentinization of abyssal peridotites at mid-ocean ridges, *C. R. Geosci.*, *335*(10–11), 825–852.
- Milliken, K. L., and J. K. Morgan (1996), Chemical evidence for near-seafloor precipitation of calcite in serpentinites (Site 897) and serpentinite breccias (Site 899), Iberia Abyssal Plain, *Proc. Ocean Drill. Program Sci. Results*, *149*, 553–558.

- Monchoux, P. (1970), Les lherzolites pyrénéennes: Contribution à l'étude de leur minéralogie, de leur génèse et de leurs transformations (Thèse d'Etat), Univ. Toulouse, Toulouse.
- Montigny, R., B. Azambre, M. Rossy, and R. Thuzat (1986), K-Ar study of Cretaceous magmatism and metamorphism in the Pyrenees: Age and length of rotation of the Iberian peninsula, *Tectonophysics*, 129, 257–273.
- Muñoz, J. A. (1992), Evolution of a continental collision belt: ECORS-Pyrenees crustal balanced cross-section, in *Thrust Tectonics*, edited by Chapman and Hall, pp. 235–246, K. McClay, London.
- O'Neil, J. R., R. N. Clayton, and T. K. Mayeda (1969), Oxygen isotope fractionation in divalent metal carbonate, *J. Chem. Phys.*, 51, 5547–5558.
- Pedreira, D., J. A. Pulgar, J. Gallart, and J. Díaz (2003), Seismic evidence of Alpine crustal thickening and wedging from the western Pyrenees to the Cantabrian Mountains (north Iberia), *J. Geophys. Res.*, 108(B4), 2204, doi:10.1029/2001JB001667.
- Pedreira, D., J. A. Pulgar, J. Gallart, and M. Torné (2007), Three-dimensional gravity and magnetic modeling of crustal indentation and wedging in the western Pyrenees-Cantabrian Mountains, *J. Geophys. Res.*, 112, B12405, doi:10.1029/2007JB005021.
- Pedreira, D., J. C. Afonso, J. A. Pulgar, J. Gallastegui, A. Carballo, M. Fernández, D. García-Castellanos, I. Jiménez-Munt, J. Semprich, and O. García-Moreno (2015), Geophysical-petrological modeling of the lithosphere beneath the Cantabrian Mountains and the North-Iberian margin: Geodynamic implications, *Lithos*, 230, 46–68, doi:10.1016/j.lithos.2015.04.018.
- Peter, J. M., and W. C. Shanks (1992), Sulfur, carbon, and oxygen isotope variations in submarine hydrothermal deposits of Guaymas Basin, Gulf of California, USA, *Geochim. Cosmochim. Acta*, 56, 2025–2040.
- Pflug, R. (1973), El Diapiro de Estella, *Soc. Cienc. Nat. Aranzadi, Num.*, 2–4(1907), 171–202.
- Quesnel, B., P. Gautier, P. Boulvais, M. Cathelineau, P. Maurizot, D. Cluzel, M. Ulrich, S. Guillot, S. Lesimple, and C. Couteau (2013), Syn-tectonic, meteoric water-derived carbonation of the New Caledonia Peridotite Nappe, *Geology*, 41(10), 1063–1066, doi:10.1130/G34531.1
- Roca, E., J. A. Muñoz, O. Ferrer, and N. Ellouz (2011), The role of the Bay of Biscay Mesozoic extensional structure in the configuration of the Pyrenean orogen: Constraints from the MARCONI deep seismic reflection survey, *Tectonics*, 30, TC2001, doi:10.1029/2010TC002735.
- Rosenbaum, G., G. S. Lister, and C. Duboz (2002), Relative motions of Africa, Iberia and Europe during Alpine orogeny, *Tectonophysics*, 359, 117–129.
- Rossy, M. (1988), Contribution à l'étude du magmatisme mésozoïque du Domain Pyrénéen: I—le Trias dans l'ensemble du domaine; II—le Crétacé dans le provinces basques d'Espagne, thesis doctoral, 429 pp., Univ. Besançon, France.
- Satish-Kumar, M. (2001), Metamorphic fluid evolution of marbles from East-Gondwana: A stable isotope perspective, *Gondwana Res.*, 4(4), 772–773.
- Schmid, T. W., and S. M. Bernasconi (2010), An automated method for “clumped-isotope” measurements on small carbonate samples, *Rapid Commun. Mass Spectrom.*, 24, 1955–1963, doi:10.1002/rcm.
- Schwarzenbach, E. M., G. L. Früh-Green, S. M. Bernasconi, J. C. Alt, and A. Plas (2013), Serpentinization and carbon sequestration: A study of two ancient peridotite-hosted hydrothermal systems, *Chem. Geol.*, 351, 115–133, doi:10.1016/j.chemgeo.2013.05.016.
- Shackleton, N. J., and J. P. Kennett (1975), Paleotemperature history of the Cenozoic and the initiation of Antarctic glaciation: Oxygen and carbon isotope analyses in DSDP Sites 277, 279, and 281, *Initial Rep. Deep Sea Drill. Proj.*, 29, 743–755.
- Shanks, W. C., III, J. K. Böhlke, and R. R. Seal II (1995), Stable isotopes in mid-ocean ridge hydrothermal systems: Interactions between Fluids, Minerals, and Organisms, in *Seafloor Hydrothermal Systems: Physical, Chemical, Biological, and Geological Interactions*, *Geophys. Monogr.*, vol. 91, No. 4, edited by S. E. Humphris, pp. 194–221, AGU, Washington, D. C., doi:10.1029/GM091p0194.
- Souquet, P., E.-J. Debroas, J.-M. Boirie, P. Pons, G. Fixari, J. Dol, J.-P. Thieuloy, M. Bonnemaïson, H. Manivit, and B. Peybernés (1985), Le groupe du Flysch noir (albo-cénomaniens) dans les Pyrénées, *Bull. Cent. Rech. Explor. Prod. Elf-Aquitaine, Pau*, 9(1), 183–252.
- Srivastava, S. P., H. Schouten, W. R. Roest, K. D. Klitgord, L. C. Kovacs, J. Verhoef, and R. Macnab (1990), Iberian plate kinematics: A jumping plate boundary between Eurasia and Africa, *Nature*, 344, 756–759.
- Stoll, H., A. Mendez-Vicente, S. Gonzalez-Lemos, A. Moreno, I. Cacho, H. Cheng, and R. L. Edwards (2015), Interpretation of orbital scale variability in mid-latitude speleothem $\delta^{18}\text{O}$: Significance of growth rate controlled kinetic fractionation effects, *Quat. Sci. Rev.*, 127, 215–228, doi:10.1016/j.quascirev.2015.08.025
- Streit, E., P. Kelemen, and J. Eiler (2012), Coexisting serpentine and quartz from carbonate-bearing serpentinized peridotite in the Samail Ophiolite, Oman, *Contrib. Mineral. Petrol.*, 164(5), 821–837, doi:10.1007/s00410-012-0775-z.
- Sumner, K. K., E. R. Camp, K. W. Huntington, T. T. Cladouhos, and M. Uddenberg (2015), Assessing fracture connectivity using stable and clumped isotope geochemistry of calcite cements, in *Proceedings, Fortieth Work. Geothermal Reserv. Eng.*, Stanford Univ., Stanford, Calif., January 26–28. SGP-TR-204.
- Swanson, E. M., B. P. Wernicke, J. M. Eiler, and S. Losh (2012), Temperatures and fluids on faults based on carbonate clumped-isotope thermometry, *Am. J. Sci.*, 312(1), 1–21, doi:10.2475/01.2012.01.
- Teixell, A., P. Labaume, and Y. Lagabrielle (2016), The crustal evolution of the west-central Pyrenees revisited: Inferences from a new kinematic scenario, *C. R. Geosci.*, 348(3–4), 257–267, doi:10.1016/j.crte.2015.10.010.
- Ternet, Y., M. Colchen, E.-J. Debroas, B. Azambre, F. Debron, J.-L. Bouchez, G. Gleizes, D. Leblanc, M. Bakalowicz, G. Jauzion, A. Mangin, and J.-C. Soulé (1997), *Note Explicative, Carte Géol. France (1/50000), feuille Aulus les Bains (1086)*, Carte géologique par M. Colchen et al. (1997), BRGM, Orléans, 146 pp.
- Trommsdorff, V., B. W. Evans, and H. R. Pfeifer (1980), Ophicarbonates rocks: Metamorphic reactions and possible origin, *Arch. Sci. Genève*, 33, 361–364.
- Tugend, J., G. Manatschal, N. J. Kusznir, E. Masini, G. Mohn, and I. Thinin (2014), Formation and deformation of hyperextended rift systems: Insights from rift domain mapping in the Bay of Biscay Pyrenees, *Tectonics*, 33, 1239–1276, doi:10.1002/2014TC003529.
- Tugend, J., G. Manatschal, and N. J. Kusznir (2015), Spatial and temporal evolution of hyperextended rift systems: Implication for the nature, kinematics, and timing of the Iberian-European plate boundary, *Geology*, 43(1), 15–18, doi:10.1130/G36072.1.
- Valley, J. W. (1986), Stable isotope geochemistry of metamorphic rocks, *Rev. Mineral. Geochem.*, 16(1), 445–489.
- Vauchez, A., C. Clerc, L. Bestani, Y. Lagabrielle, A. Chauvet, A. Lahfid, and D. Mainprice (2013), Preorogenic exhumation of the North Pyrenean Agly massif (Eastern Pyrenees-France), *Tectonics*, 32, 95–106, doi:10.1002/tect.20015.
- Vergés, J., H. Millán, E. Roca, J. A. Muñoz, M. Marzo, J. Cirés, T. Den Bezemer, R. Zoetemeijer, and S. Cloetingh (1995), Eastern Pyrenees and related foreland basins: Pre-, syn- and post-collisional crustal-scale cross-sections, *Mar. Pet. Geol.*, 12(8), 893–915.
- Walgenwitz, F. (1976), Étude pétrologique des roches intrusives triasiques, des écaïlles de socle profond et des gîtes de chlorite de la région d'Elizondo (Navarre, Espagne), Thèse 3ème cycle, Besançon, 17. Université de Franche-Comté, France.